α-Glucosidase Inhibitors from *Preussia minimoides*

By: Manuel Rangel-Grimaldo, Isabel Rivero-Cruz, Abraham Madariaga-Mazón, Mario Figueroa, and Rachel Mata

Rangel-Grimaldo, M., Rivero-Cruz, I., Madariaga-Mazón, A., Figueroa, M., Mata, R. (2017). α-Glucosidase Inhibitors from Preussia minimoides. *Journal of Natural Products, 80* (3), pp. 582-587. DOI: 10.1021/acs.jnatprod.6b00574

Abstract:

Extensive fractionation of an extract from the grain-based culture of the endophytic fungus *Preussia minimoides* led to the isolation of two new polyketides with novel skeletons, minimoidiones A (**1**) and B (**2**), along with the known compounds preussochromone C (**3**), corymbiferone (**4**), and 5-hydroxy-2,7-dimethoxy-8-methylnaphthoquinone (**5**). The structures of **1** and **2** were elucidated using 1D and 2D NMR data analysis, along with DFT calculations of ^{1}H NMR chemical shifts. The absolute configuration of **1** was established by a single-crystal X-ray diffraction analysis and TDDFT-ECD calculations. Compounds **1**–**4** significantly inhibited yeast α-glucosidase.

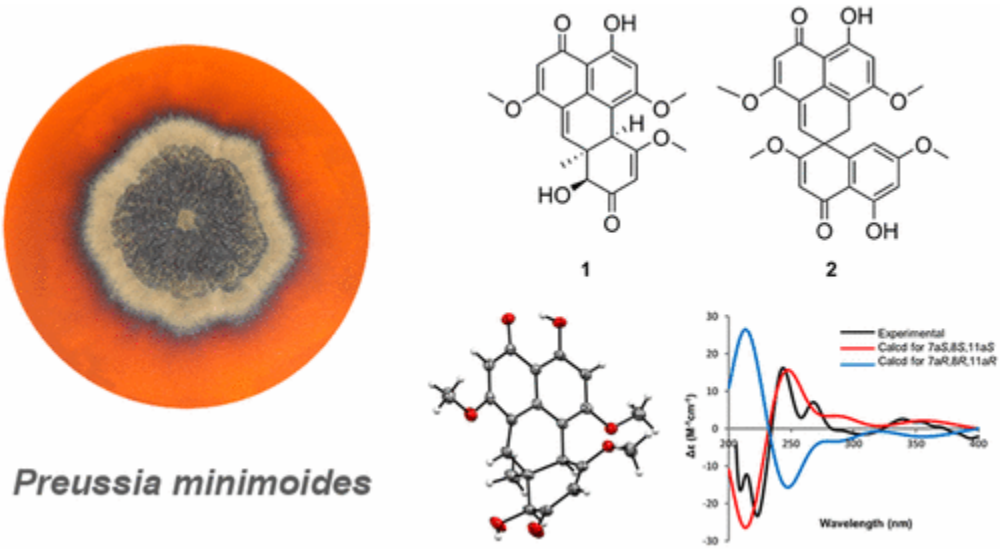

Keywords: *Preussia minimoides* | polyketides | antidiabetic drugs | diabetes treatment

Article:

The genus *Preussia* (Sporormiaceae) comprises species isolated from soil, wood, and plant debris. *Sporormiella* Ellis & Everh. is a similar genus, defined originally to include exclusively coprophilous species. Recent studies have demonstrated no difference between the two genera with respect to their habitat and other diagnostic morphological features. Thus, some authors consider it more appropriate to treat them as synonyms.(1, 2) *Preussia minimoides* (S.I. Ahmed & Cain) Valldos. & Guarro (Sporormiaceae) [Syn: *Sporormiella minimoides* S.I. Ahmed & Cain] is a prolific producer of many interesting polyketides and depsipeptides.(3) Some of these metabolites possess interesting biological activities, including cytotoxicity (brocaenol A),(4) antibacterial and antifungal activities (sporminarins A and B),(5) and calmodulin inhibitory effects (corymbiferone C, corymbiferan lactone E, and 5-hydroxy-2,7-dimethoxy-8-methylnaphthoquinone).(6)

The search for new α-glucosidase inhibitors and other antidiabetic drugs from natural sources has increased notably in recent years, considering that type II diabetes mellitus is one of the most challenging health problems of the 21st century. Therefore, as part of an effort to discover new α-glucosidases inhibitors useful for the development of antidiabetic drugs, we now report the isolation and structure elucidation of two new polyketides with novel skeletons, namely, minimoidiones A (**1**) and B (**2**), from an endophytic isolate of the fungus *P. minimoides* obtained from *Hintonia latiflora* (Sessé et Mociño ex DC.) Bullock (Rubiaceae).(6)

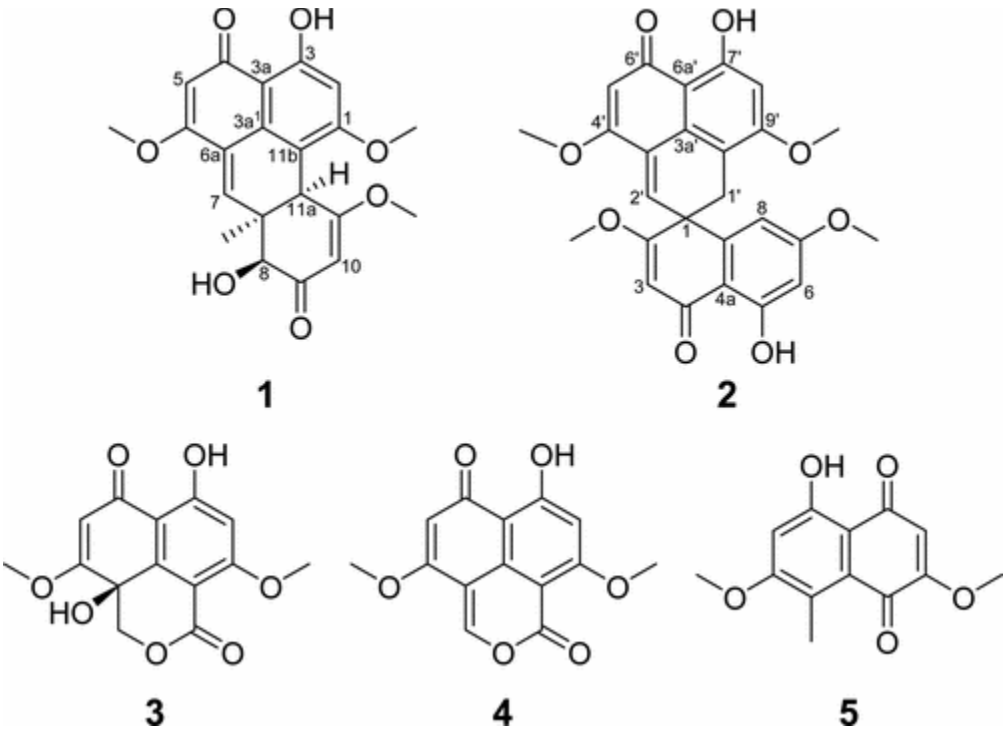

Results and Discussion

The defatted extract from moist rice cultures of *P. minimoides* inhibited the activity of yeast α-glucosidase (αGHY) with an IC_{50} of 38 μg/mL. Extensive fractionation of this extract yielded two novel polyketides, the benzo[*de*]anthracenedione **1** and the spiro[naphthalenephenalene]dione **2**, which were given the trivial names minimoidiones A and

B, respectively. In addition, the known compounds preussochromone C (**3**),(7) corymbiferone (**4**),(8) and 5-hydroxy-2,7-dimethoxy-8-methylnaphthoquinone (**5**)(6) were isolated. Compound **3** was isolated for the first time from *P. minimoides*, and its NMR data were identical to those previously reported. Compounds **4** and **5** were previously obtained from the same isolate and were characterized by comparison with authentic samples.(6)

Minimoidione A (**1**) was isolated as yellow crystals. Its molecular formula, $C_{21}H_{20}O_7$, established from HRESIMS data, indicated a structure with 12 degrees of unsaturation. The IR (1651 cm^{-1}) and UV (maxima at 205, 221, 260, and 301 nm) spectra revealed absorptions indicative of conjugated ketone and aromatic moieties. Analysis of the ^1H and ^{13}C NMR data indicated the presence of 21 carbon atoms consisting of three methoxy groups, one additional methyl, six methines (four in the aromatic-vinylic region and two aliphatic), 11 nonprotonated carbons (two conjugated ketones, eight aromatic or olefinic, and one aliphatic), and two hydroxy groups (Table 1). On the basis of the 1D and 2D NMR data (Figures S4–S7), two partial substructures of **1** (**a** and **b**; Figure 1) were elucidated. Rings A and B of substructure **a** were assigned considering the HMBC correlations from H-2 to C-1/C-3/C-3a and from H-5 to C-3a/C-4/C-6/C-6a; the NOESY cross-peaks between H-2 and 1-OCH_3 and from H-5 to 6-OCH_3; and the presence of a phenolic hydroxy group at δ_H 13.21 (3-OH), which was chelated with the conjugated ketone group at δ_C 190.4 (C-4). On the other hand, diagnostic chemical shifts for the presence of a second α,β unsaturated ketone system and the HMBC correlations from H-10 to C-8/C-9/C-11/C-11a, from H-8 to C-7/C-7a/C-9/7a-CH_3, and from H-11a to C-10/C-11/C-11b assembled ring D of substructure **b** (Figure 1). Consideration of the molecular formula indicated that these partial structures have to be linked to form an additional ring (ring C). HMBC correlations from H-11a (δ_H 4.28) to C-1 (δ_C 163.4 in ring A)/C-10 (δ_C 100.4 at ring D)/C-11 (δ_C 175.1 at ring D)/C-11b (δ_C 108.9 at ring A) and from H-7 (δ_H 6.98, ring C) to C-6a/C-7a/C-8/C-11a (Figure 1) confirmed this tetracyclic system. Altogether, these correlations resulted in the planar structure of compound **1**. The NOESY (Figure S6) interactions between 7a-CH_3, H-8, and H-11a indicated that they had the same relative orientation. An X-ray diffraction analysis of **1** with Mo Kα radiation confirmed the proposed structure and the relative configuration at the chiral centers. An ORTEP drawing of the crystallographically determined structure of **1** is depicted in Figure 2.

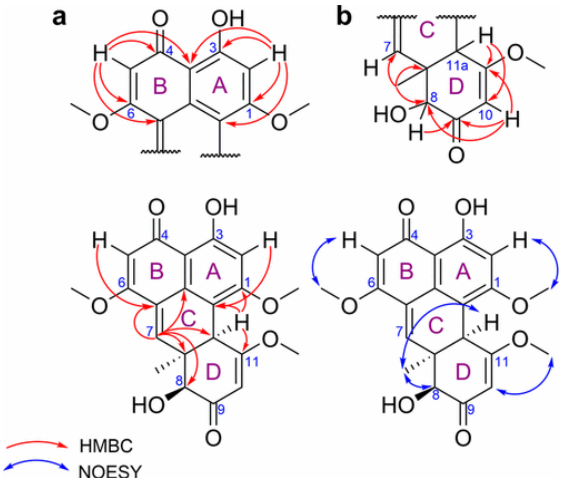

Figure 1. Partial structures **a** and **b** and selected HMBC and key NOESY correlations of minimoidione A (**1**).

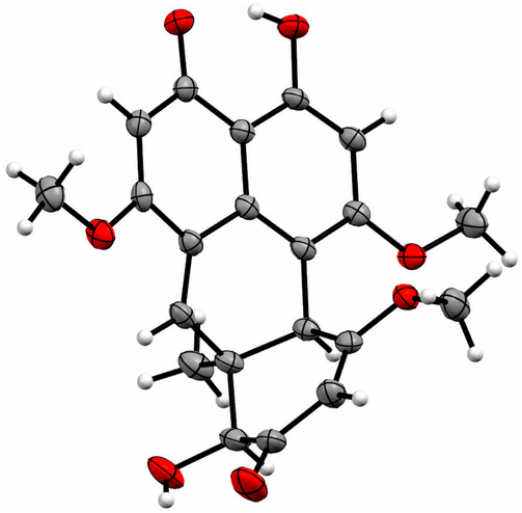

Figure 2. ORTEP drawing of compound **1**.

Table 1. ^{1}H (500 MHz) and ^{13}C (125 MHz) NMR Data for Compound 1 in $CDCl_3$

position	δ_C, type		δ_H (*J* in Hz)	HMBC	NOESY
1	163.4	C			
2	99.2	CH	6.49, s	1, 3, 3a, 11b	1-OCH_3
3	163.1	C			
3a	106.8	C			
3a[1]	130.5	C			
4	190.4	C			
5	101.4	CH	5.65, s	3a, 4, 6, 6a	6-OCH_3
6	165.1	C			
6a	125.9	C			
7	138.4	CH	6.98, d (1.5)	3a[1], 6, 7a, 8, 11a	
7a	44.1	C			
8	76.6	CH	4.25, s	7, 7a, 7a-CH_3, 9	7a-CH_3
9	196.6	C			
10	100.4	CH	5.50, d (2.0)	8, 9, 11, 11a	11-OCH_3
11	175.1	C			
11a	41.4	CH	4.28, t (2.0)	1, 10, 11, 11b	7a-CH_3
11b	108.9	C			
1-OCH_3	55.9	CH_3	3.90, s	1	2
6-OCH_3	55.8	CH_3	3.80, s	6	5
11-OCH_3	56.8	CH_3	3.53, s	11	10
7a-CH_3	20.9	CH_3	1.28, s	7, 7a, 8, 11a	8, 11a
3-OH			13.21, s	2, 3, 3a	
8-OH			5.30, s		

The absolute configuration at the stereogenic centers of **1** was deduced by comparison of the experimental and calculated electronic circular dichroism (ECD) spectra of the two possible enantiomers (7a*S*,8*S*,11a*S* and 7a*R*,8*R*,11a*R*), which were calculated using time-dependent

density functional theory (TDDFT). The calculated spectrum for the 7a*S*,8*S*,11a*S* isomer showed good agreement with the experimental data (Figure 3).

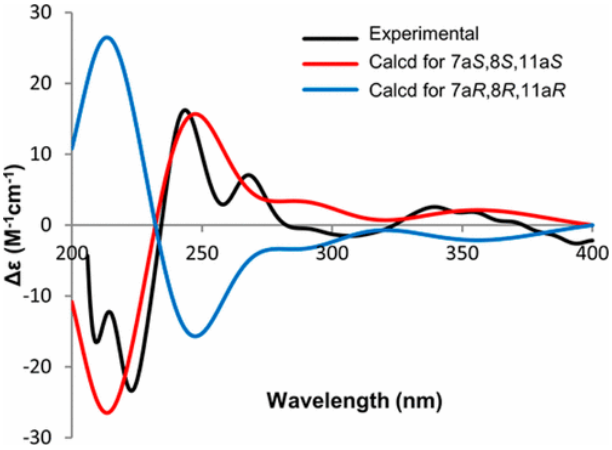

Figure 3. Comparison of the experimental ECD spectrum of **1** (black) with those calculated at the B3LYP/6-31+G(d) level for enantiomers 7a*S*,8*S*,11a*S* (red) and 7a*R*,8*R*,11a*R* (blue).

Minimoidione B (**2**) was isolated as an optically inactive orange solid that analyzed for $C_{26}H_{22}O_8$, which would require 16 double-bond equivalents. The IR spectrum showed characteristic absorptions for aromatic ring (1623 and 1461 cm^{-1}), hydroxy group (3437 cm^{-1}), and carbonyl groups (1653 cm^{-1}). The 1D and 2D NMR data (Table 2) included signals for four methoxy groups, one methylene, six aromatic or olefinic methines, and 16 nonprotonated carbons, including two conjugated ketone carbonyls, 14 aromatic, six of which were oxygenated, and one aliphatic. Finally, two phenolic chelated hydroxy groups were detected (δ_H 13.30 and 13.14). As in compound **1**, detailed analysis of the 2D NMR spectra, in particular of the HMBC data, led to partial structures **c** and **d** indicated in Figure 4. Substructure **c** (rings A and B), identical to substructure **a** of compound **1**, was elucidated on the basis of the HMBC cross-peaks from H-8′ to C-6′a/C-7′/C-9, from H-5′ to C-3′/C-4′/C-6′, and from H-2′ to C-1/C-3′/C-4′. Furthermore, the NOESY correlations from H-8′ to 9′-OCH_3 and H-5′ to 4′-OCH_3 and the chelated phenolic hydroxy group at δ_H 13.14 (7′-OH) completed the assembly. On the other hand, substructure **d** (including rings D and E and a methylene functionality) was established considering the following HMBC correlations: from H-6 to C-4a/C-5/C-7/C-8, from H-3 to C-1/C-2/C-4/C-4a, from H-8 to C-1/C-4a/C-7, and from H_2-1′ to C-1/C-2/C-8a. The AB system for two *meta*-related protons observed in the ^{1}H NMR between H-6 (δ_H 6.35, d, J = 2.5 Hz) and H-8 (δ_H 6.24, d, J = 2.5 Hz) and the NOESY correlations between H-3 and H-6 with the methoxy groups at C-2 and C-7, respectively, further supported substructure **d**. These partial structures were linked to form an additional ring (ring C), based on the unsaturation count and the HMBC correlations from H-1a′ and H-1b′ (δ_H 3.39 and 3.19, dd, J = 18 Hz) to C-2′/C-3a′/C-9′/C-10′ (Figure 4). In addition, the correlations from H-1a′ and H-1b′ to C-1, from H-2′ to C-1, from H-3 to C-1, and from H-8 to C-1 indicated that ring C was linked to ring D in a *spiro* fashion (Figure 4). The only asymmetric center of compound **2** was located at C-1, but the lack of optical activity and molecular symmetry indicated that the compound was a racemic mixture. On the basis of the above considerations, the structure of compound **2** was fully assembled.

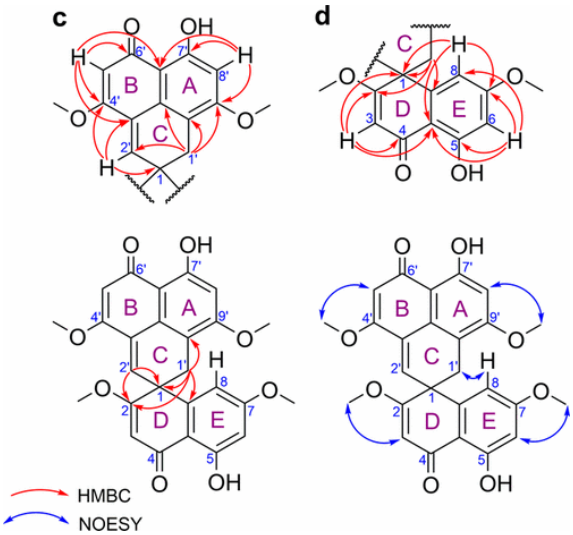

Figure 4. Partial structures **c** and **d** and selected HMBC and key NOESY correlations of minimoidione B (**2**).

Table 2. ^{1}H (500 MHz) and ^{13}C (125 MHz) NMR Data for Compound 2 in $CDCl_3$

position	δ_C, type		δ_H (*J* in Hz)	HMBC	NOESY
1	44.6	C			
2	177.8	C			
3	100.6	CH	5.70, s	1, 2, 4, 4a	2-OCH_3
4	189.7	C			
4a	106.7	C			
5	164.6	C			
6	99.9	CH	6.35,d (2.5)	4a, 5, 7, 8	7-OCH_3
7	164.7	C			
8	106.4	CH	6.24, d (2.5)	1, 4a, 6, 7	7-OCH_3, 1′
8a	129.2	C			
2-OCH_3	56.7	OCH_3	3.80, s	2	3
7-OCH_3	55.4	OCH_3	3.67, s	7	6, 8
1′	33.1	CH_2	3.39, d (18) 3.19, d (18)	1, 2, 2′, 3a′, 8a, 9′, 10′	8
2′	135.0	CH	6.67, s	1, 2, 3′, 4′	4′-OCH_3
3′	126.5	C			
3a′	147.0	C			
4′	164.8	C			
5′	102.1	CH	5.75, s	3′, 4′,6′, 6a′	4′-OCH_3
6′	190.1	C			
6a′	106.7	C			
7′	162.4	C			
8′	99.3	CH	6.45, s	7′, 6a′, 10′	9′-OCH_3
9′	161.6	C			
10′	109.8	C			
4′-OCH_3	56.0	OCH_3	3.84, s	4′	2′, 5′
9′-OCH_3	55.7	OCH_3	3.79, s	9′	8′
OH-5			13.30, s	5, 6	
OH-7′			13.14, s		

All attempts to obtain suitable crystals of **2** for X-ray analysis failed. Therefore, in order to provide further evidence for our structural assignment of **2**, ^{1}H NMR chemical shifts were

calculated and compared with the experimental data according to the protocol of Willoughby and collaborators.(9) Basically, this protocol involves a conformational search using molecular mechanics, geometry optimization using DFT, and chemical shift calculations using the GIAO method with the B3LYP/6-311+G(2d,p) level of theory. The computed ^{1}H NMR chemical shifts of compound **2** (Tables S5 and S7) were all within 0.28 ppm of the corresponding experimental values. As can be seen in Tables S5 and S8, the matched mean absolute error was <0.17 ppm.(9)

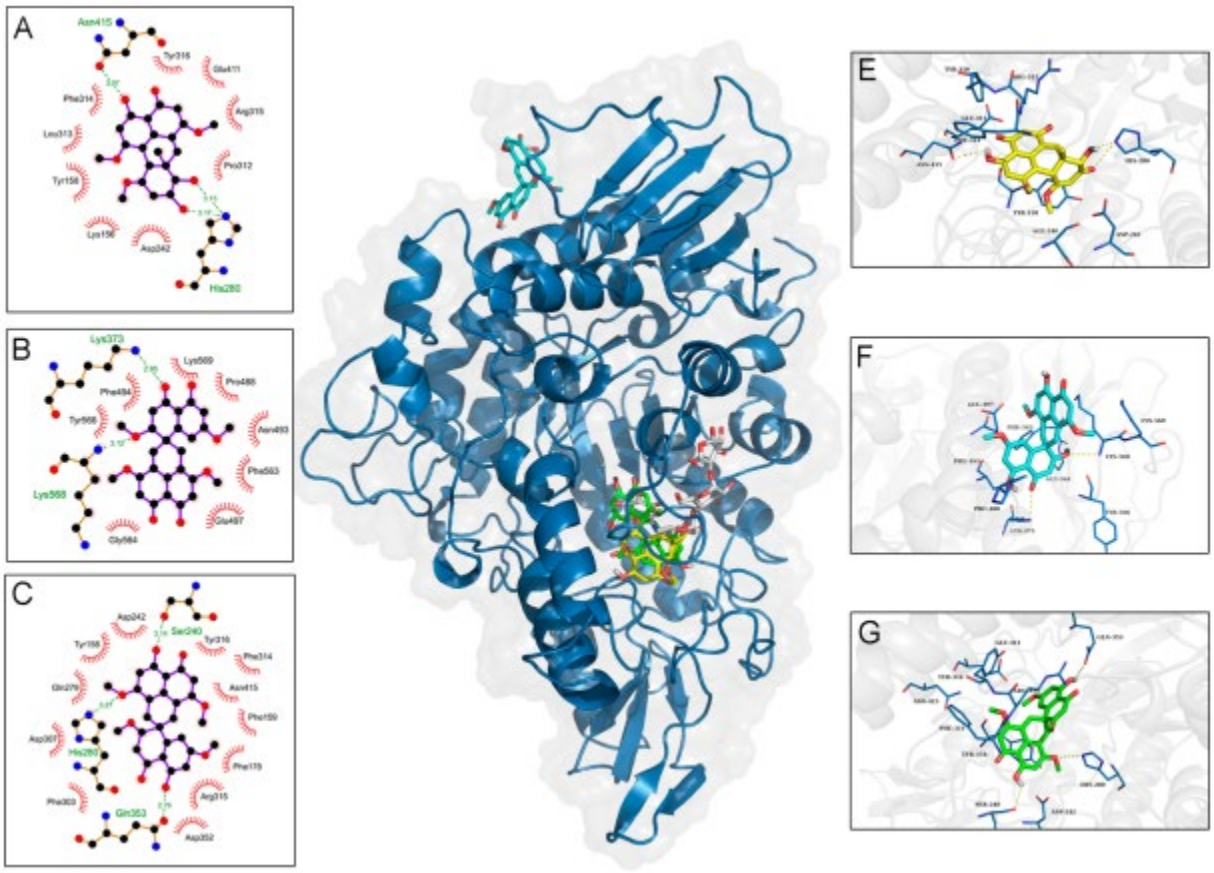

Figure 5. Model of binding for compounds **1** (yellow sticks) and the two stereoisomers of **2**, *R* (cyan sticks) and *S* (green sticks), with αGHY (blue cartoon, pdb 3A4A). The insets show details of the binding mode for **1** (A and E), **2***R* (B and F), and **2***S* (C and G).

Compounds **1**–**4** inhibited yeast α-glucosidase (αGHY), with IC_{50}'s ranging from 2.9 to 155 μM (Table S9). Among them, compound **2** showed the strongest effect (IC_{50} = 2.9 μM). In all cases, the activity was compared to that of an acarbose standard (IC_{50} = 877 μM). In order to envisage the putative binding mode of compounds **1** and **2** with αGHY, docking analyses were carried out using the crystallized structure of αGHY (pdb code 3A4A).(10, 11) The docking protocol was validated reproducing the binding mode of acarbose at the catalytic domain (Figure S23).(12, 13) Next, minimiodione A (**1**) and the *R* and *S* enantiomers of **2** were docked into the validated α-glucosidase model. The results predicted that the *R* enantiomer of compound **2** binds in a site different from the catalytic domain [binding energy (ΔG) = −7.7 kcal/mol]. This site was composed mainly by hydrophobic interactions including Pro488, Asn493, Phe494, Glu497, Phe563, Gly564, Tyr566, and Lys569 and hydrogen bonds between Lys373 and Lys568 (Figure 5C and F). On the other hand, docking of compound **1** and the *S* stereoisomer of **2** suggested that

they bind to the catalytic site of αGHY with higher affinities (ΔG = −8.5 and −10.4 kcal/mol, respectively). The interactions in this site included hydrophobic contacts with Tyr158, Asp242, Phe314, Arg315, Tyr316, Glu411, and Asn415 and hydrophilic interactions with Ser240, His280, and Gln353 (Figure 5A, E, C, and G).

Experimental Section

General Experimental Procedures

Melting points were determined on a Fisher-Johns apparatus and are uncorrected. IR, UV, and ECD spectra were obtained on a PerkinElmer 400 FT-IR, a Shimadzu U160, and a JASCO model J720 spectrophotometer, respectively. Optical rotations were recorded at the sodium D-line wavelength using a PerkinElmer model 343 polarimeter at 20 °C. 1D and 2D NMR spectra were recorded on a 400 MHz Bruker Avance III (operating at 400 MHz for ^{1}H and 100 MHz for ^{13}C), a Varian Inova 300 MHz (operating at 300 MHz for ^{1}H and 75 MHz for ^{13}C), or a Varian Unity Inova 500 MHz (operating at 500 MHz for ^{1}H and 125 MHz for ^{13}C) spectrometer; spectra were recorded using $CDCl_3$ and tetramethylsilane as an internal standard. HRESIMS spectra were obtained using a Thermo LTQ Orbitrap XL mass spectrometer.

ESIMS analyses were performed on an SQD2 single-quadrupole mass spectrometer with an electrospray ion source. Data acquisition and processing was accomplished with the MassLynx software version 4.1 (Waters). HPLC was carried out on a Waters system equipped with a 2535 pump and a 2998 photodiode array detector; data acquisition and management of chromatographic output were performed with the Empower 3 software (Waters). Reagent-grade dichloromethane, *n*-hexane, and methanol and HPLC-grade acetonitrile and methanol (J.T. Baker) were regularly used in the extraction and isolation procedures. Silica gel 60 (70–230 mesh, Merck) and Sephadex LH-20 (General Electric) were used for column chromatography (CC). TLC analyses were performed on precoated silica gel 60 F_{254} plates (Merck) using different mobile phases, and visualization of plates was carried out using a 10% $Ce(SO_4)_2$ solution in H_2SO_4 and heating.

Isolation and Identification of *P. minimoides*

The endophytic fungus *P. minimoides* was isolated from selected adult and healthy leaves of *H. latiflora*, collected by Sol Cristians in Huetamo (18°31.709′ N, 101°4.692′ W; 221 masl), State of Michoacan, Mexico, on July 2010. Identification of the plant was secured by the collector; a voucher specimen (131 336) was deposited at the Herbario de la Facultad de Ciencias (FCME), Mexico City, Mexico. The fungus was isolated as previously described.(6) The pure fungal strain was obtained after serial transfers on PDA plates and deposited into the Herbario Nacional de México (MEXU, voucher number 26355). The fungus was identified based on morphological characteristics, such as ascospore morphology.(6) Sequence data [internal transcribed spacer (ITS) and 28S rRNA] were deposited in GenBank as accessions KF557658 and KF557659, respectively. Data available at GenBank aligning with MEXU 26355 suggested this fungus is *P. minimoides.*

Fermentation, Extraction, and Isolation

Erlenmeyer flasks with 50 mL of potato-dextrose broth (Difco) sterilized by autoclaving at 121 °C for 15 min were individually inoculated with 1 cm^3 agar taken from a stock culture of *P. minimoides* on PDA plates. Cultures grown for 1 week were used to inoculate eight 2.8 L Fernbach flasks containing solid rice medium (200 g of white rice and 400 mL of H_2O). *P. minimoides* was cultured at room temperature for 45 days in static conditions with a 12/12 h daily light–dark period. After incubation, the solid medium was extracted exhaustively with a mixture of CH_2Cl_2–MeOH (8:2) via maceration. The extract was dried over Na_2SO_4 (anhydrous) and concentrated in vacuo to yield 7.3 g of a brownish oily residue. The extract was reconstituted with MeOH–MeCN (1:1) and partitioned with *n*-hexane to yield two primary fractions. The MeOH–MeCN fraction (5.4 g) inhibited the activity of the yeast α-glucosidase with an IC_{50} of 38 μg/mL, and it was further fractionated via silica gel column chromatography, eluting with a gradient of *n*-hexane–CH_2Cl_2 (100:0 → 0:100) and CH_2Cl_2–MeOH (100:0 → 80:20) to afford nine secondary fractions (F1–F9). Fraction F6 (184.8 mg) was subjected to Sephadex LH-20 CC eluting with CH_2Cl_2–MeOH (8:2) to afford six fractions (F_6I–F_6VI). Fraction F_6IV (71.5 mg) was further purified by reversed-phase HPLC (Gemini C_{18}, 250 × 21.24 mm, 5 μm, Phenomenex) using as mobile phase 30:70 MeCN–H_2O (acidified with 0.1% formic acid) and increasing linearly to 50% MeCN over 30 min and finally to 100% MeCN for 5 min, at a flow rate of 21.24 mL/min. This process yielded 5.6 mg of **1** as yellow needles. Fraction F4 (184.8 mg) was first washed with *n*-hexane (80 mL); the resulting residue (107.3 mg) was further purified by reversed-phase HPLC (Gemini C_{18}, 250 × 21.24 mm, 5 μm, Phenomenex) using as mobile phase 60:40 MeCN–H_2O (acidified with 0.1% formic acid) and increasing linearly to MeCN over 15 min, at a flow rate of 21.24 mL/min; this procedure afforded 11.6 mg of **2** as an orange solid and 20.3 mg of **4** as a yellow powder.

Fraction F9 (425.9 mg) was purified by silica gel chromatography with a gradient of Hex–AcOEt (100:0 → 0:100) and AcOEt–MeOH (100:0 → 70:30) to afford seven fractions (F_9I– F_9VII). Fraction F_9IV (48.8 g) was further purified by reversed-phase CC (Gemini C_{18}, 250 × 21.24 mm, 5 μm, Phenomenex) using as mobile phase 70:30 MeCN–H_2O (acidified with 0.1% formic acid) and increasing linearly to 50% MeCN over 30 min, at a flow rate of 21.24 mL/min, to obtain 3.2 mg of **3** as a yellow, amorphous solid. Fraction F2 (68.2 mg) was washed with *n*-hexane (30 mL) and then was subjected to Sephadex LH-20 chromatography eluting with CH_2Cl_2–MeOH (8:2) to afford five fractions (F_2I–F_2V). From fraction F_2IV spontaneously precipitated 16.3 mg of **5** as an orange powder.

Minimoidione A (1):

($C_{21}H_{20}O_7$) yellow needles; mp 230–232 °C; $[\alpha]^{20}_D$ +27.17 (1 mg/mL, $CHCl_3$); UV (MeOH, *c* 1.8) λ_{max} (log ε) 221 (−3.8), 243 (1.8), 258 (−0.1), 268 (0.3), 316 (−0.6) nm; IR (FTIR) ν_{max} 3640, 3119, 1670, 1616, 1246 cm^{-1}; ^1H and ^{13}C NMR in Table 1; HRESIMS *m*/*z* 385.1270 $[M + H]^+$, calcd 385.1282.

Minimoidione B (2):

($C_{26}H_{22}O_8$) orange solid; mp 280–281 °C; $[\alpha]^{20}_D$ 0 (1 mg/mL, $CHCl_3$); IR (FTIR) ν_{max} 3065, 3916, 2956, 1633, 1587, 1572, 1229, 1214 cm^{-1}; ^1H and ^{13}C NMR in Table 2; HRESIMS *m/z* 463.1375 $[M + H]^+$, calcd 463.1387.

X-ray Crystal Structure Analysis of Compound 1

Single crystals suitable for X-ray analysis were obtained by recystallization from $CHCl_3$–MeOH (8:2). A yellow crystal having approximate dimensions of 0.273 × 0.118 × 0.076 mm was mounted on a glass fiber. All measurements were made on a Bruker Smart Apex CCD diffractometer equipped with graphite-monochromated Mo Kα radiation (λ = 0.710 73 Å) at 150 K. The structure was solved by the SHELXS-2013 method and refined using full-matrix least-squares on F^2. Suitable crystals of **1** were obtained by evaporation of CH_2Cl_2–MeOH (8:2). Crystallographic data for **1** have been deposited with the Cambridge Crystallographic Data Centre (CCDC) with the accession no. 1475816. These data are available, free of charge, from the CCDC via http://www.ccdc.cam.ac.uk/data_request/cif.

Crystal data for 1:

$C_{21}H_{20}O_7$, MW 384.37, monoclinic, space group $P2_1/n$, with unit cell parameters a = 9.1302(13) Å, b = 15.476(2) Å, c = 13.420(2) Å, α = 90°, β = 109.085(3)°, γ = 90°, Z = 4, T = 150(2) K, volume 1792.0(4) $Å^3$, F(000) 808, density(calcd) 1.425 Mg/m^3. Intensity data were collected in the range of 2.382–25.193° using a ω scan; 10 832 reflections collected, 3193 independent reflections [R(int) = 0.1193] were considered, observed, and used in the calculations. The final R_1 values were 0.0568 [$I > 2\sigma(I)$]. The final $wR_2(F^2)$ values were 0.1138 [$I > 2\sigma(I)$], with a data–restraints–parameters ratio of 3193/2/263. The final R_1 values were 0.1021 (all data). The final $wR_2(F^2)$ values were 0.1404 (all data).

Computational Section

Minimum energy structures for the different stereoisomers were built with Spartan'08 software (Wavefunction Inc.). Conformational analysis was performed with the Monte Carlo search protocol as implemented in the same software under the MMFF94 molecular mechanics force field. The resulting conformers were minimized using the DFT method at the B3LYP/6-311+G(2d,p) level of theory for NMR chemical shift prediction. NMR shielding tensors were computed with the gauge-independent atomic orbital (GIAO) method and the polarizable continuum model using the integral equation formalism variant (IEFPCM) as the SCRF method.(9) The TDDFT method at the B3LYP/6-31+G(d) level of theory was employed for ECD calculations using the same DFT-minimized conformers. The self-consistent reaction field with conductor-like continuum solvent model was used to perform the ECD calculations of the major conformers of both **1** enantiomers in MeOH. The calculated excitation energy (nm) and rotatory strength (R) in dipole velocity (R_{vel}) and dipole length (R_{len}) forms were simulated into an ECD curve. All calculations were performed employing the Gaussian'09 program package (Gaussian Inc.).

The minimized structures for docking simulations were prepared using Autodock Tools package v1.5.4 (ADT, http://mgltools.scripps.edu/).(14) For metabolites, addition of Gasteiger charges

and number of torsions were set, and nonpolar hydrogens were merged. The crystallographic structure of α-glucosidase from yeast was obtained from the Protein Data Bank (RCSB; pdb code 3A4A). For the receptor all hydrogens (polar and nonpolar) and Kollman charges were added, and solvation parameters were assigned by default.

Molecular docking studies were achieved with AutoDock Vina v1.1.2.(15) First, a blind docking was performed in order to establish the common site of interaction of the metabolites with the α-glucosidase. The search space for this preliminary docking was defined as a box size of 54 × 68 × 68 Å in the *x*, *y*, and *z* dimensions, with a grid spacing of 1.0 Å and the macromolecule set as the center of the box. The default parameters of exhaustiveness and number of modes were not altered. Next, a refined docking was performed with a smaller box of searching space (30 × 25 × 25 Å and 1.0 Å of grid spacing), setting as the center of the grid box the lower state pose obtained from the blind docking. The conformational states from the docking simulations were analyzed using the AutoDockTools program, which also identified the H-bonds and van der Waals interactions between the catalytic site of α-glucosidase and the ligand. The predicted docked complexes (protein–ligand) were those conformations showing the lowest binding energy. The estimated inhibition constant (K_i) was calculated from the docking energy displayed by AutoDock Vina following the equation $K_i = \exp(\Delta G \times 1000/RT)$, where ΔG is the docking energy, R is the universal constant of an ideal gas (1.987 19 cal K^{-1} mol^{-1}), and T is the temperature (298.15 K). Preparation of the figures was accomplished with the PyMOL visualization tool (PyMOL Molecular Graphics System, version 1.7.4, Schrödinger, LLC)(16) and LigPlot$^+$.(17)

Assay for α-Glucosidase Inhibitors

The fungal extract, fractions, compounds, and acarbose (positive control) were dissolved in MeOH. Aliquots of 0–40 μL of testing materials (triplicated) were incubated for 10 min with 20 μL of enzyme stock solution (0.4 units/mL in phosphate buffer solution 100 mM, pH 7). After incubation, 10 μL of substrate (*p*NPG 5 mM) was added and further incubated for 30 min at 37 °C,(18) and the absorbances were determined. For the extract and fractions, the inhibitory activity was determined as a percentage in comparison to the blank (MeOH) according to the following equation: $$\%\ \alpha\mathrm{GHY} = \left(1 - \frac{A_{415t}}{A_{415c}}\right) \times 100\%$$ where % αGHY is the percentage of inhibition, A_{415t} is the corrected absorbance of the extract, fractions, or compound under testing ($A_{415\ \mathrm{end}} - A_{415\ \mathrm{initial}}$), and A_{415c} is the absorbance of the blank ($A_{415\ \mathrm{end\ blank}} - A_{415\ \mathrm{initial\ blank}}$). The IC_{50} was calculated by regression analysis, using the following equation: $$\%\ \mathrm{Inhibition} = \frac{A_{100}}{1 + \left(\frac{I}{IC_{50}}\right)^s}$$ where A_{100} is the maximum inhibition, I is the inhibitor concentration, IC_{50} is the concentration required to inhibit activity of the enzyme by 50%, and s is the cooperative degree.(19)

Supporting Information

The Supporting Information is available free of charge on the ACS Publications website at DOI: 10.1021/acs.jnatprod.6b00574.

1D and 2D NMR spectra of compounds **1**–**5**, X-ray crystallographic data of **1**, calculated DFT B3LYP/6-31+G(d) free energies, population and theoretical averaged rotatory strength values expressed in $R_{(len)}$ for conformers of 7a*R*,8*R*,11a*R* and 7a*S*,8*S*,11a*S* enantiomers of **1**, comparison of computed and experimental ^{1}H NMR data for **1** and **2** (*S* and *R* enantiomers), and inhibitory effect of **14** evaluated with αGHY (PDF)

The authors declare no competing financial interest.

‡Taken in part from the Ph.D. thesis of Manuel Rangel-Grimaldo.

Dedicated to Professor Phil Crews, of the University of California, Santa Cruz, for his pioneering work on bioactive natural products.

Acknowledgment

This work was supported by grants from CONACyT CB 219765, CONACyT INFRA 252226, and PAIP-UNAM 5000-9140. We thank R. del Carmen for his valuable technical assistance. M.R.-G. acknowledges a fellowship from CONACyT (234569) to pursue graduate studies. We are indebted to Dirección General de Cómputo y de Tecnologías de Información y Comunicación (DGTIC), UNAM, for providing the resources to carry out computational calculations through the Miztli supercomputing system.

References

1. Arenal, F.; Platas, G.; Peláez, F. Mycotaxon **2004**, 89, 137– 151

2. Arenal, F.; Platas, G.; Peláez, F. Fungal Divers. **2005**, 20, 1– 15

3. Clapp-Shapiro, W. H.; Burgess, B. W.; Giacobbe, R. A.; Harris, G. H.; Mandala, S.; Polishook, J.; Rattray, M.; Thornton, R. A.; Zink, D. L.; Cabello, A.; Diez, M. T.; Martin, I.; Pelaez, F. U.S. Patent 5,801,172 A, 1998.

4. Bugni, T. S.; Bernan, V. S.; Greenstein, M.; Janso, J. E.; Maiese, W. M.; Mayne, C. L.; Ireland, C. M. J. Org. Chem. **2003**, 68, 2014– 2017 DOI: 10.1021/jo020597w

5. Mudur, S. V.; Gloer, J. B.; Wicklow, D. T. J. Antibiot. **2006**, 59, 500– 506 DOI: 10.1038/ja.2006.70

6. Leyte-Lugo, M.; Figueroa, M.; González, M.; del, C.; Glenn, A. E.; González-Andrade, M.; Mata, R. Phytochemistry **2013**, 96, 273– 278 DOI: 10.1016/j.phytochem.2013.09.006

7. Zhang, F.; Li, L.; Niu, S.; Si, Y.; Guo, L.; Jiang, X.; Che, Y. J. Nat. Prod. **2012**, 75, 230– 237 DOI: 10.1021/np2009362

8. Overy, D. P.; Zidorn, C.; Petersen, B. O.; Duus, J. Ø.; Dalsgaard, P. W.; Larsen, T. O.; Phipps, R. K. Tetrahedron Lett. **2005**, 46, 3225– 3228 DOI: 10.1016/j.tetlet.2005.03.043

9. Willoughby, P. H.; Jansma, M. J.; Hoye, T. R. Nat. Protoc. **2014**, 9, 643– 660 DOI: 10.1038/nprot.2014.042

10. Morris, G. M.; Goodsell, D. S.; Halliday, R. S.; Huey, R.; Hart, W. E.; Belew, R. K.; Olson, A. J. J. Comput. Chem. **1998**, 19, 1639– 1662 DOI: 10.1002/(SICI)1096-987X(19981115)19:14<1639::AID-JCC10>3.0.CO;2-B

11. Rudnitskaya, A.; Török, B.; Török, M. Biochem. Mol. Biol. Educ. **2010**, 38, 261– 265DOI: 10.1002/bmb.20392

12. Yamamoto, K.; Nakayama, A.; Yamamoto, Y.; Tabata, S. Eur. J. Biochem. **2004**, 271, 3414– 3420 DOI: 10.1111/j.1432-1033.2004.04276.x

13. Rivera-Chávez, J.; Figueroa, M.; González, M.; del, C.; Glenn, A. E.; Mata, R. J. Nat. Prod. **2015**, 78, 730– 735 DOI: 10.1021/np500897y

14. Morris, G. M.; Huey, R.; Lindstrom, W.; Sanner, M. F.; Belew, R. K.; Goodsell, D. S.; Olson, A. J. J. Comput. Chem. **2009**, 30, 2785– 2791 DOI: 10.1002/jcc.21256

15. Trott, O.; Olson, A. J. J. Comput. Chem. **2010**, 31, 455– 461

16. Seeliger, D.; de Groot, B. L. J. Comput.-Aided Mol. Des. **2010**, 24, 417– 422 DOI: 10.1007/s10822-010-9352-6

17. Wallace, A. C.; Laskowski, R. A.; Thornton, J. M. Protein Eng., Des. Sel. **1995**, 8, 127– 134 DOI: 10.1093/protein/8.2.127

18. Rivera-Chávez, J.; González-Andrade, M.; González, M.; del, C.; Glenn, A. E.; Mata, R. Phytochemistry **2013**, 94, 198– 205 DOI: 10.1016/j.phytochem.2013.05.021

19. Copeland, R. A. Enzymes: A Practical Introduction to Structure, Mechanism, and Data Analysis, 2nd ed.; Wiley-VCH: Weinheim, Germany, **2000**; p 416.

α-Glucosidase Inhibitors from *Preussia minimoides*‡

Manuel Rangel-Grimaldo†*, Isabel Rivero-Cruz, Abraham Madariaga-Mazón, Mario Figueroa and Rachel Mata**

Facultad de Química, Universidad Nacional Autónoma de México, Ciudad de Mexico 04510, México.

SUPPORTING INFORMATION

List of Contents

Figure S18. ^{13}C NMR spectrum of corymbiferone (**4**) in $CDCl_3$.

Figure S19. ^{1}H NMR spectrum of 5-hydroxy-2,7-dimethoxy-8-methylnaphthoquinone (**5**) in $CDCl_3$.

Figure S20. ^{13}C NMR spectrum of 5-hydroxy-2,7-dimethoxy-8-methylnaphthoquinone (**5**) in $CDCl_3$.

Figure S21. Calculated ECD at DFT B3LYP/6-31+G(d) theory Level for 7a*S*,8*S*,11a*S* enantiomer of **1.**

Figure S22. Calculated ECD at DFT B3LYP/6-31+G(d) theory Level for 7aR,8*R*,11a*R* enantiomer of **1.**

Figure S23. 2D Representation of the interactions among αGHY and acarbose in the predicted binding site.

Spectroscopic and spectrometric data for 3–5

Table S1. Geometry Optimization and ^{1}H NMR Single-Point Calculations at DFT B3LYP/6-311+G(2d,p) Level of Theory for Minimoidione A (**1**).

Table S2. Comparison of Computed and Experimental ^{1}H NMR Data for **1**.

Table S3. Calculated DFT B3LYP/6-31+G(d) Free Energies, Population and Theoretical Averaged Rotatory Strength Values Expressed in *R(len)* for Conformers of 7a*S*,8*S*,11a*S* Enantiomer of **1**.

Table S4. Calculated DFT B3LYP/6-31+G(d) Free Energies, Population and Theoretical Averaged Rotatory Strength Values Expressed in *R(len)* for Conformers of 7a*R*,8*R*,11a*R* Enantiomer of **1**.

Table S5. Geometry Optimization and ^{1}H NMR Single-Point Calculations at DFT B3LYP/6-311+G(2d,p) Level of Theory for ***R*** Enantiomer of Minimoidione B (**2**).

Table S6. Comparison of Computed and Experimental ^{1}H NMR Data for *R* Enantiomer of **2**.

Table S7. Geometry Optimization and ^{1}H NMR Single-Point Calculations at DFT B3LYP/6-311+G(2d,p) Level of Theory for ***S*** Enantiomer of Minimoidione B (**2**).

Table S8. Comparison of Computed and Experimental ^{1}H NMR Data for *S* Enantiomer of **2**.

Table S9. Inhibitory Effect of Compounds **1**–**4** Evaluated with αGHY.

Table S10. Crystal Data and Structure Refinement for Minimoidione A (**1**).

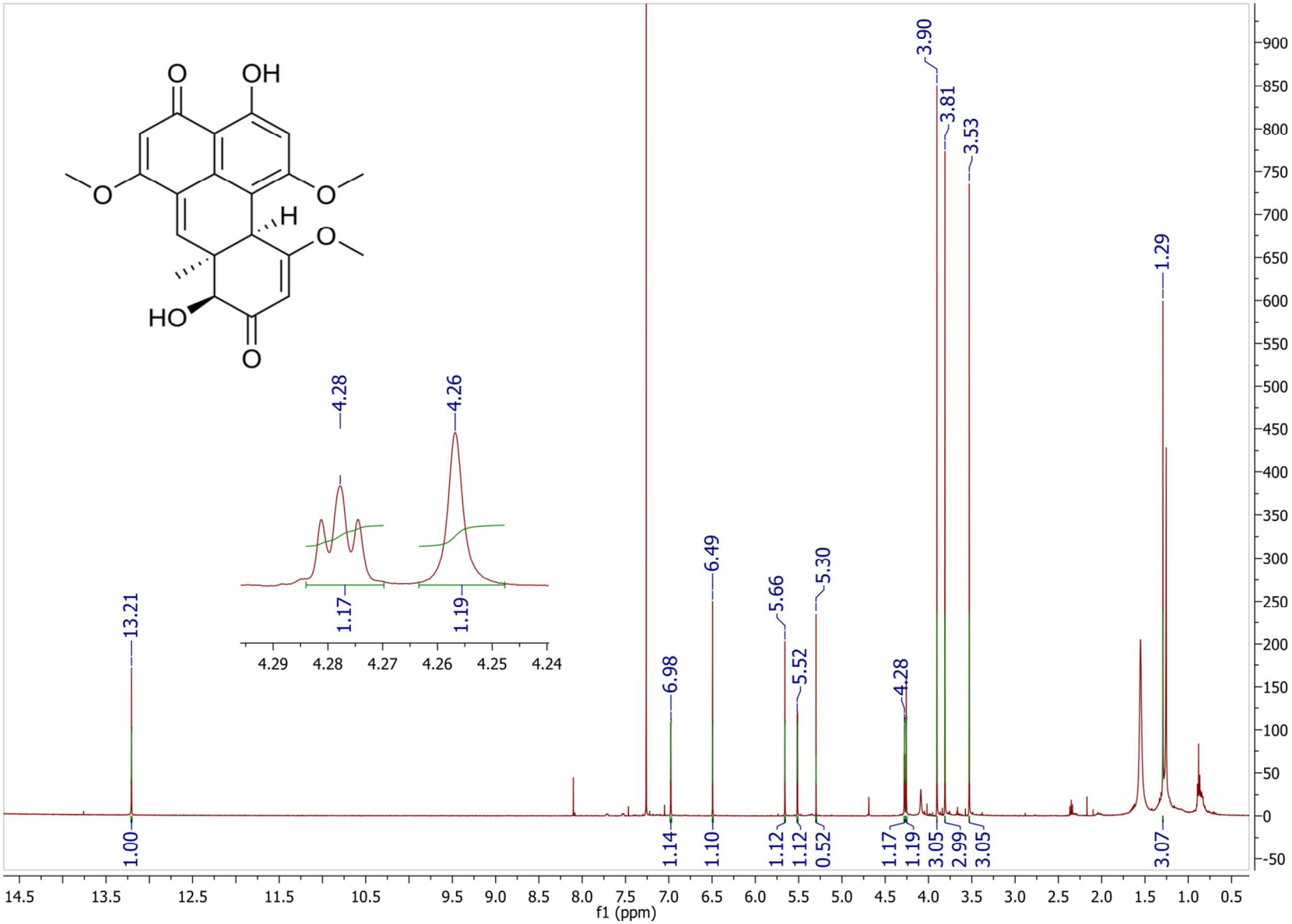

Figure S1. ^{1}H NMR spectrum of minimoidione A (**1**) in $CDCl_3$.

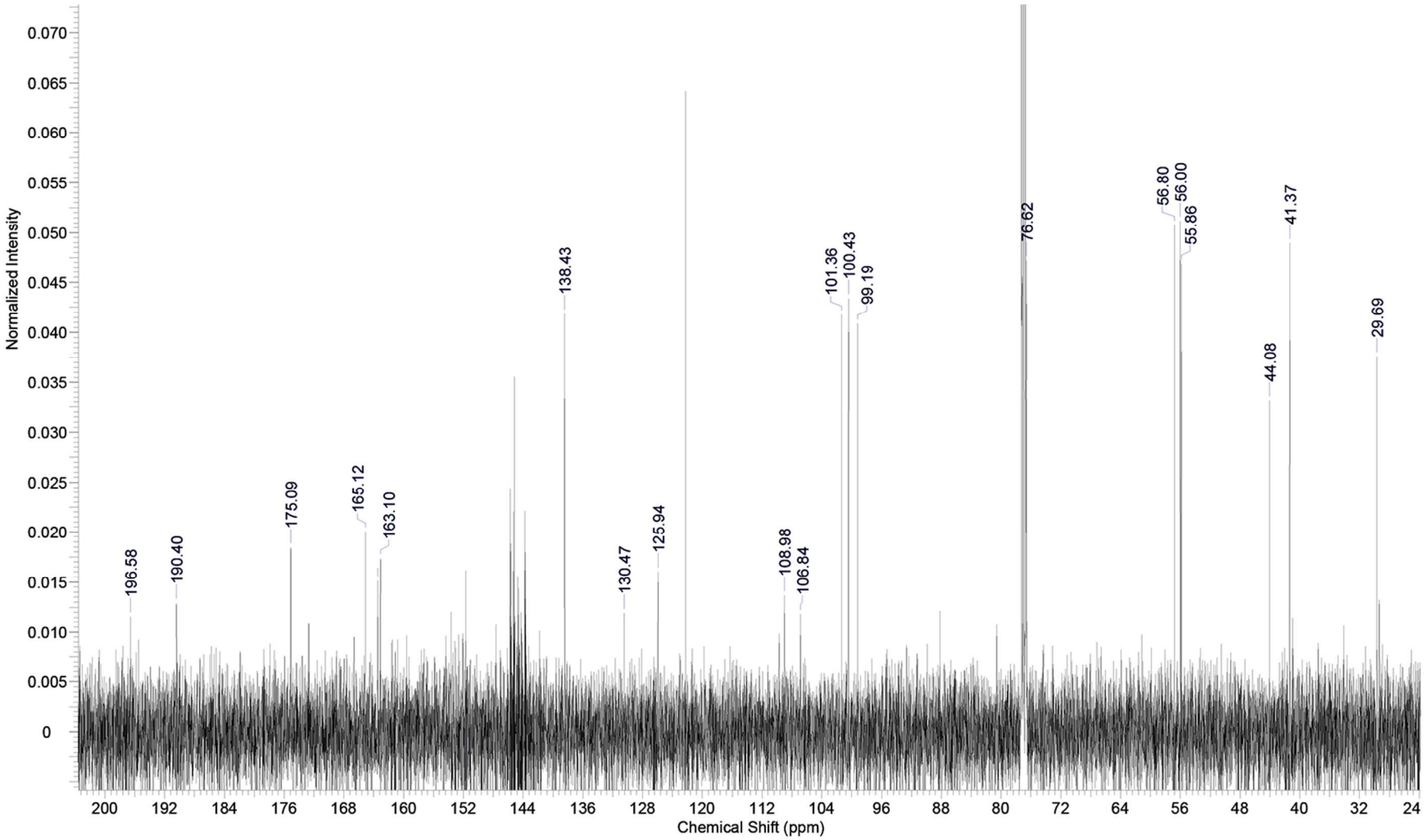

Figure S2. ^{13}C NMR spectrum of minimoidione A (**1**) in $CDCl_3$.

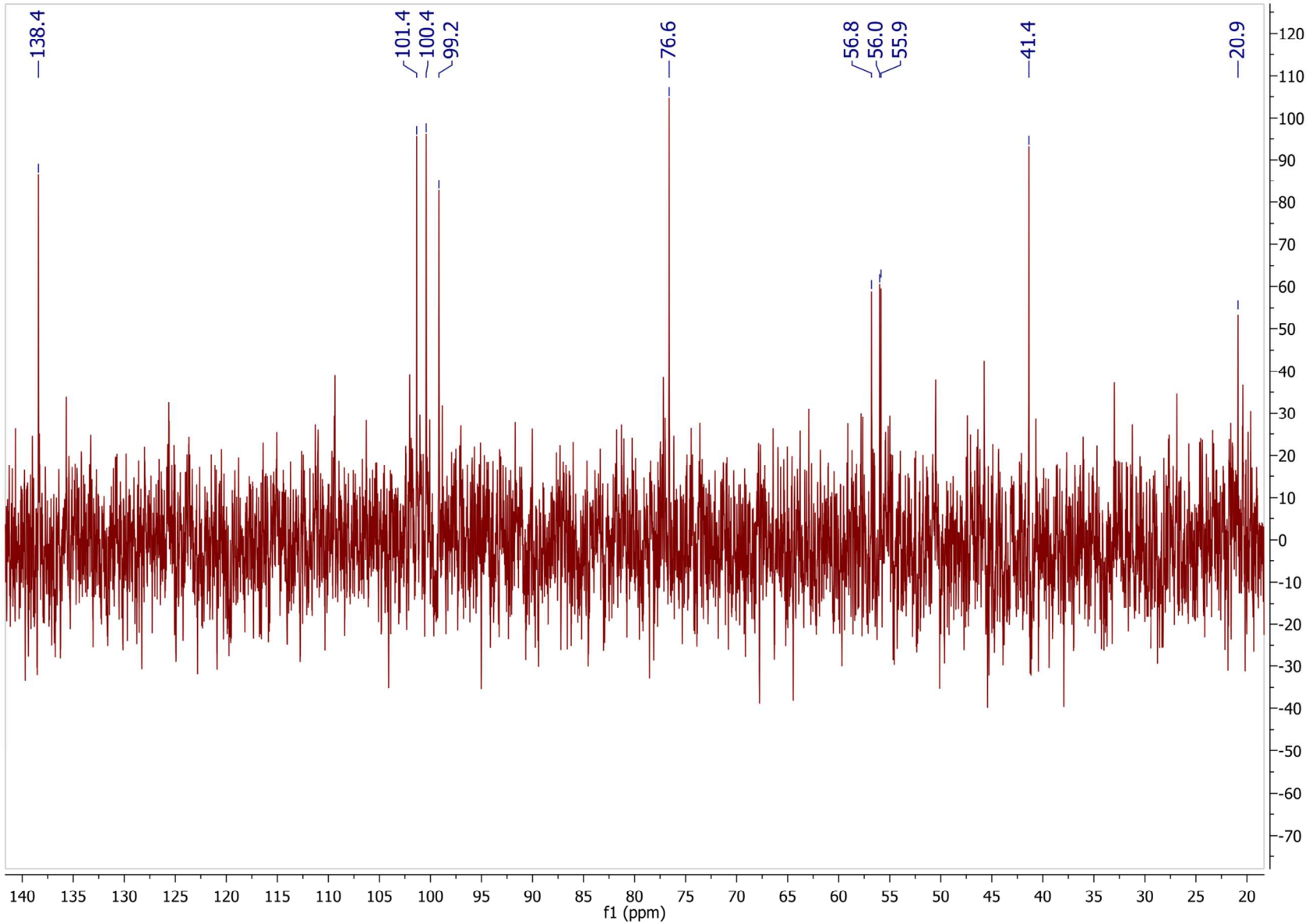

Figure S3. DEPT-135 spectrum of minimoidione A (**1**) in $CDCl_3$.

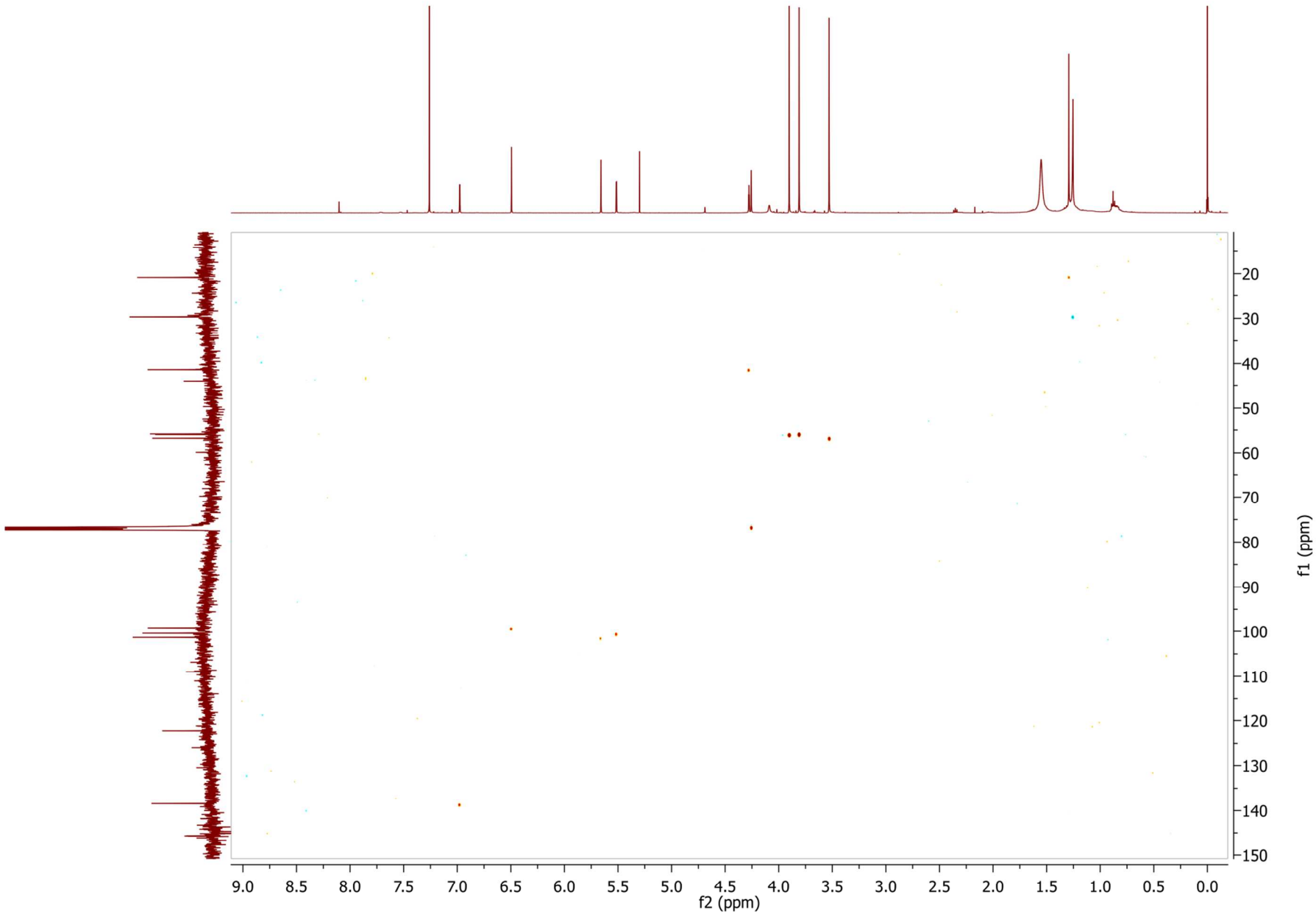

Figure S4. HSQC spectrum of minimoidione A (**1**) in $CDCl_3$.

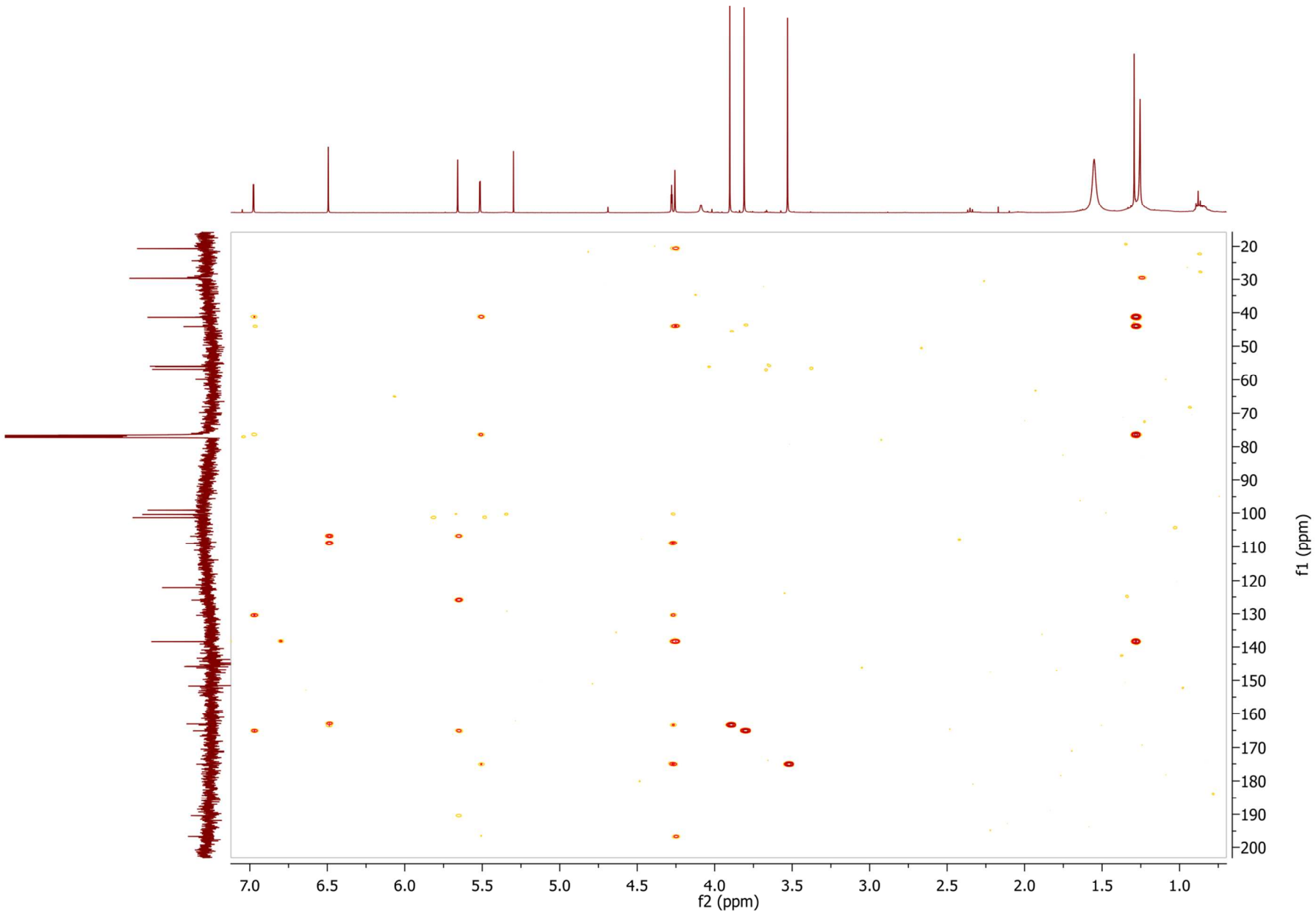

Figure S5. HMBC spectrum of minimoidione A (**1**) in $CDCl_3$.

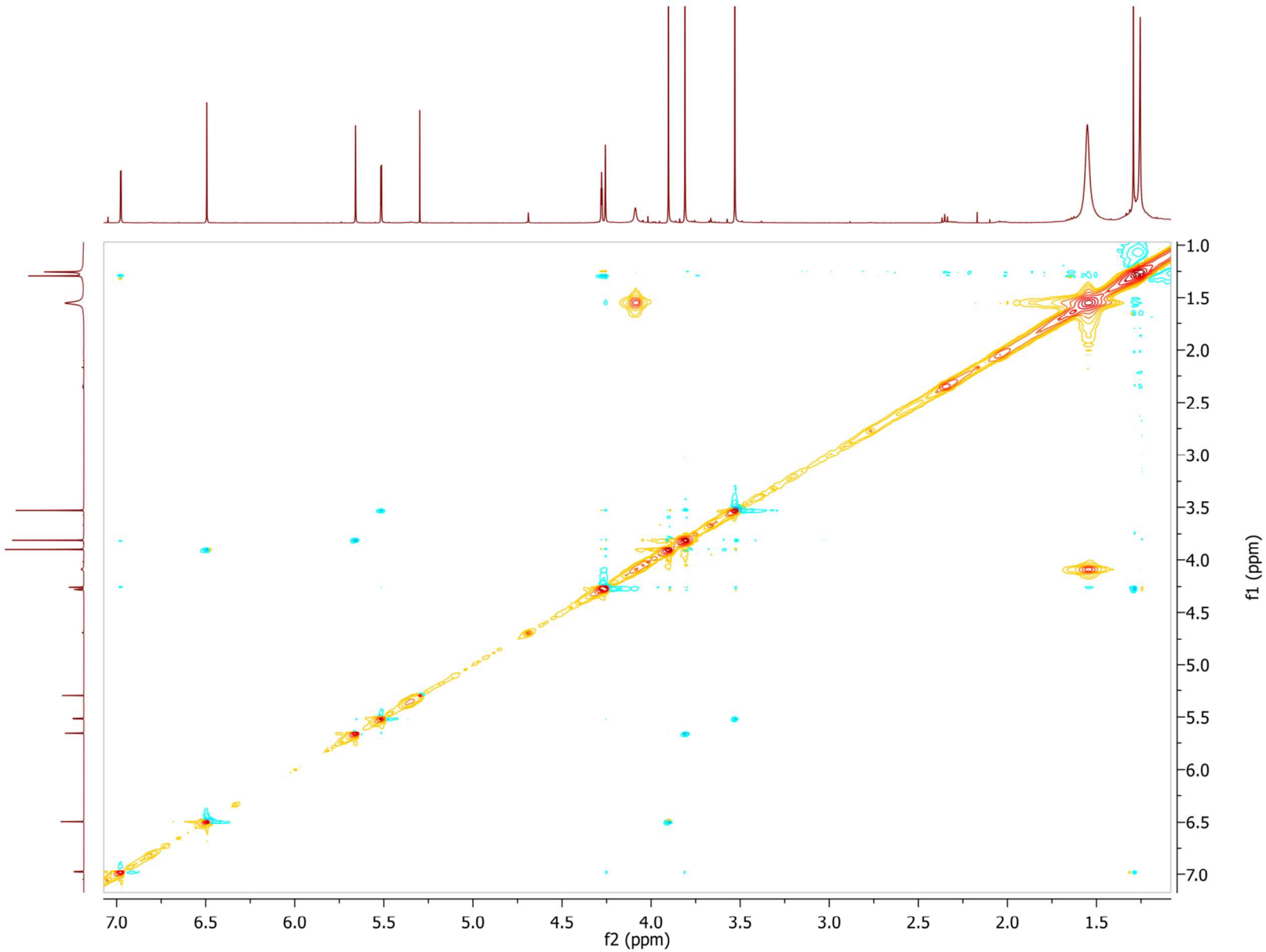

Figure S6. NOESY spectrum of minimoidione A (**1**) in $CDCl_3$.

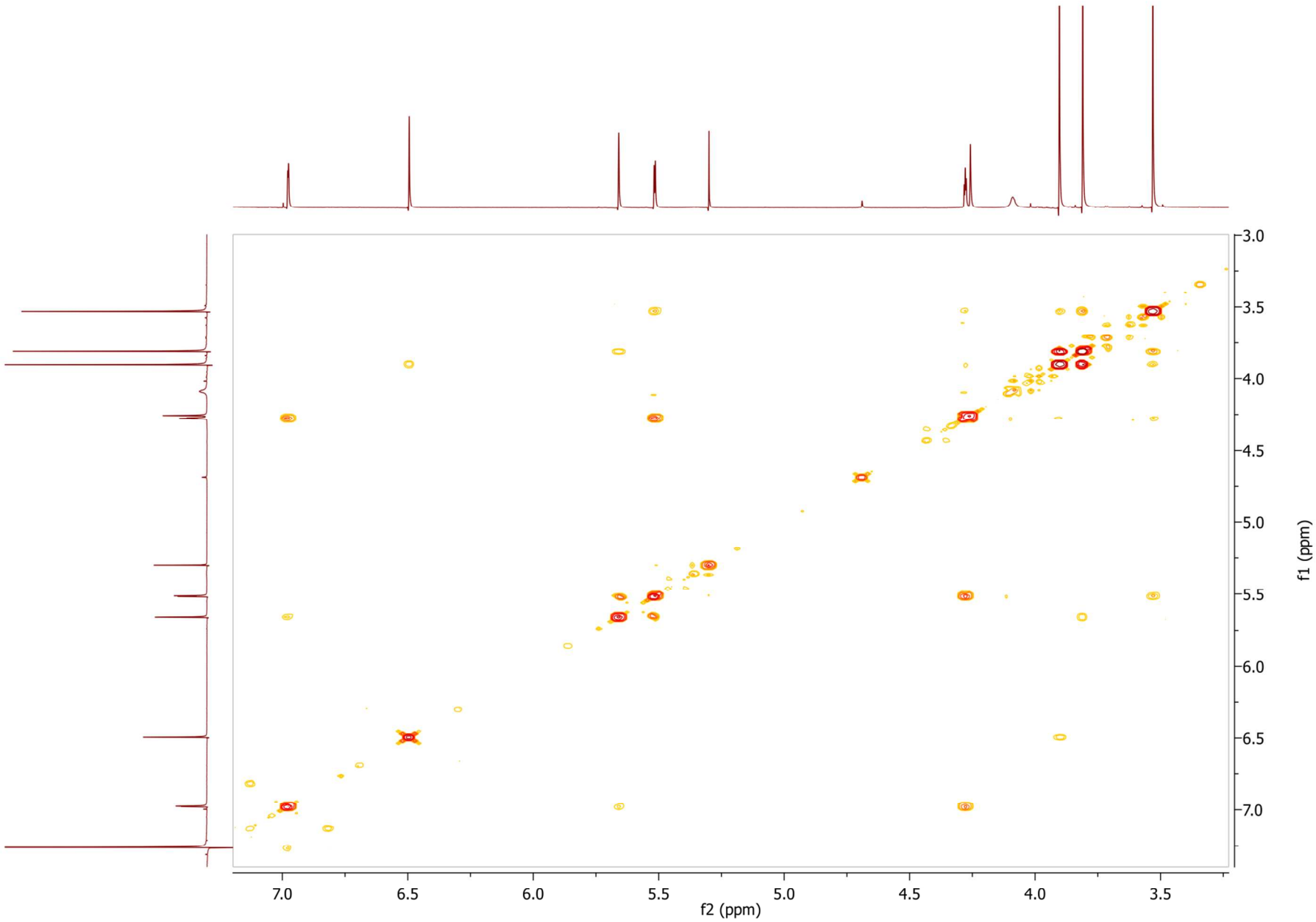

Figure S7. COSY spectrum of minimoidione A (**1**) in $CDCl_3$.

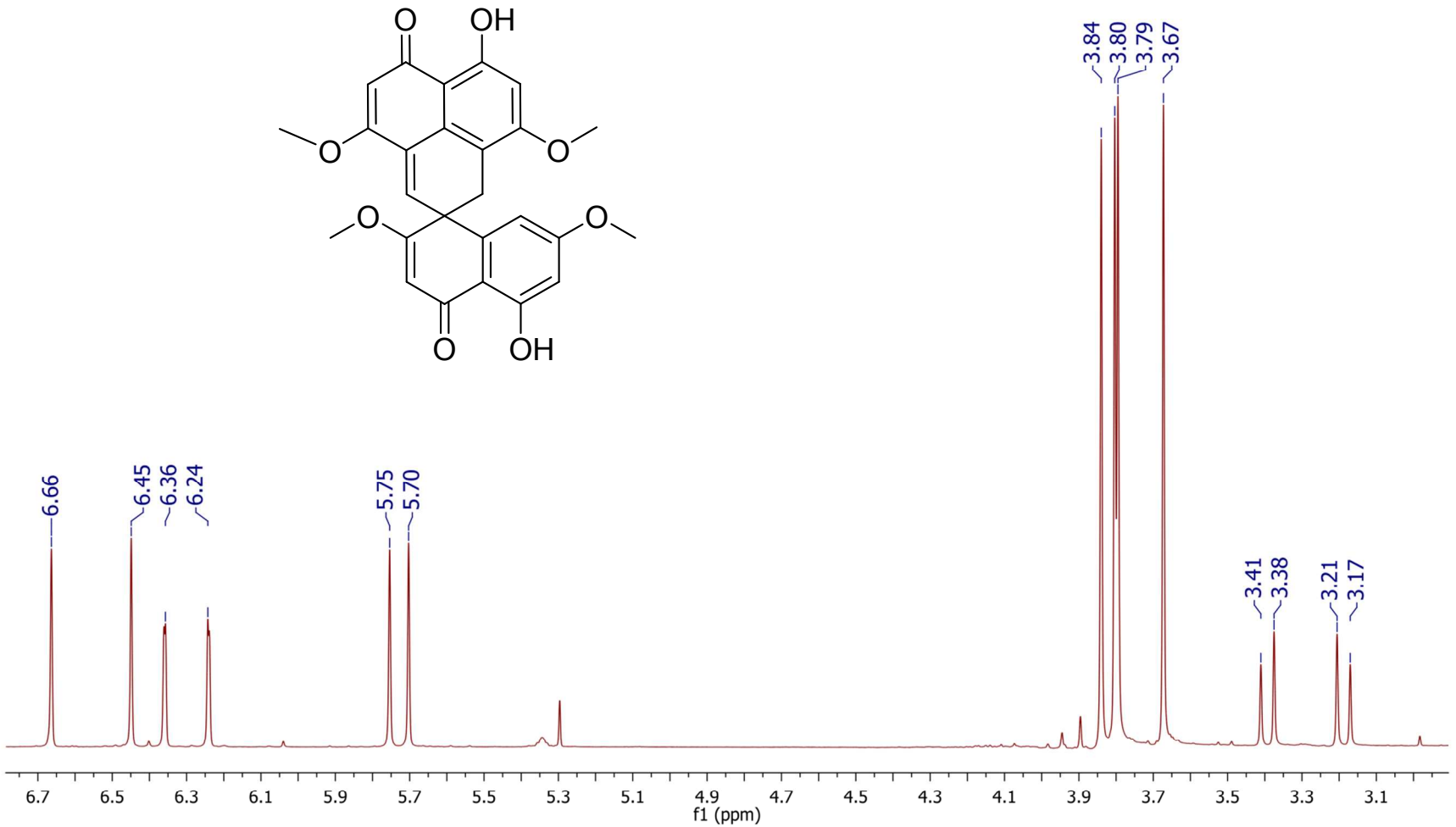

Figure S8. ^{1}H NMR spectrum of minimoidione B (**2**) in $CDCl_3$.

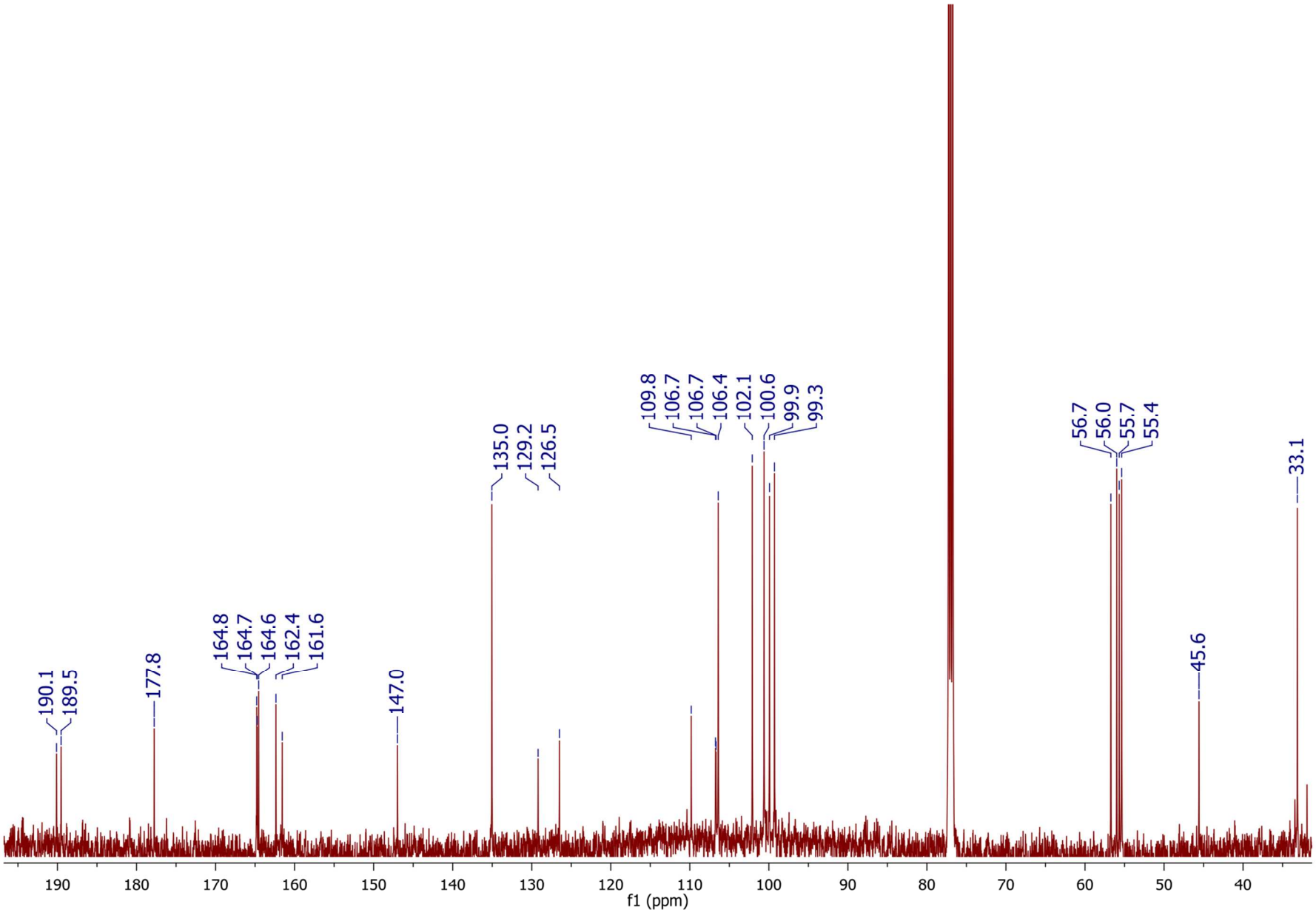

Figure S9. ^{13}C NMR spectrum of minimoidione B (**2**) in $CDCl_3$.

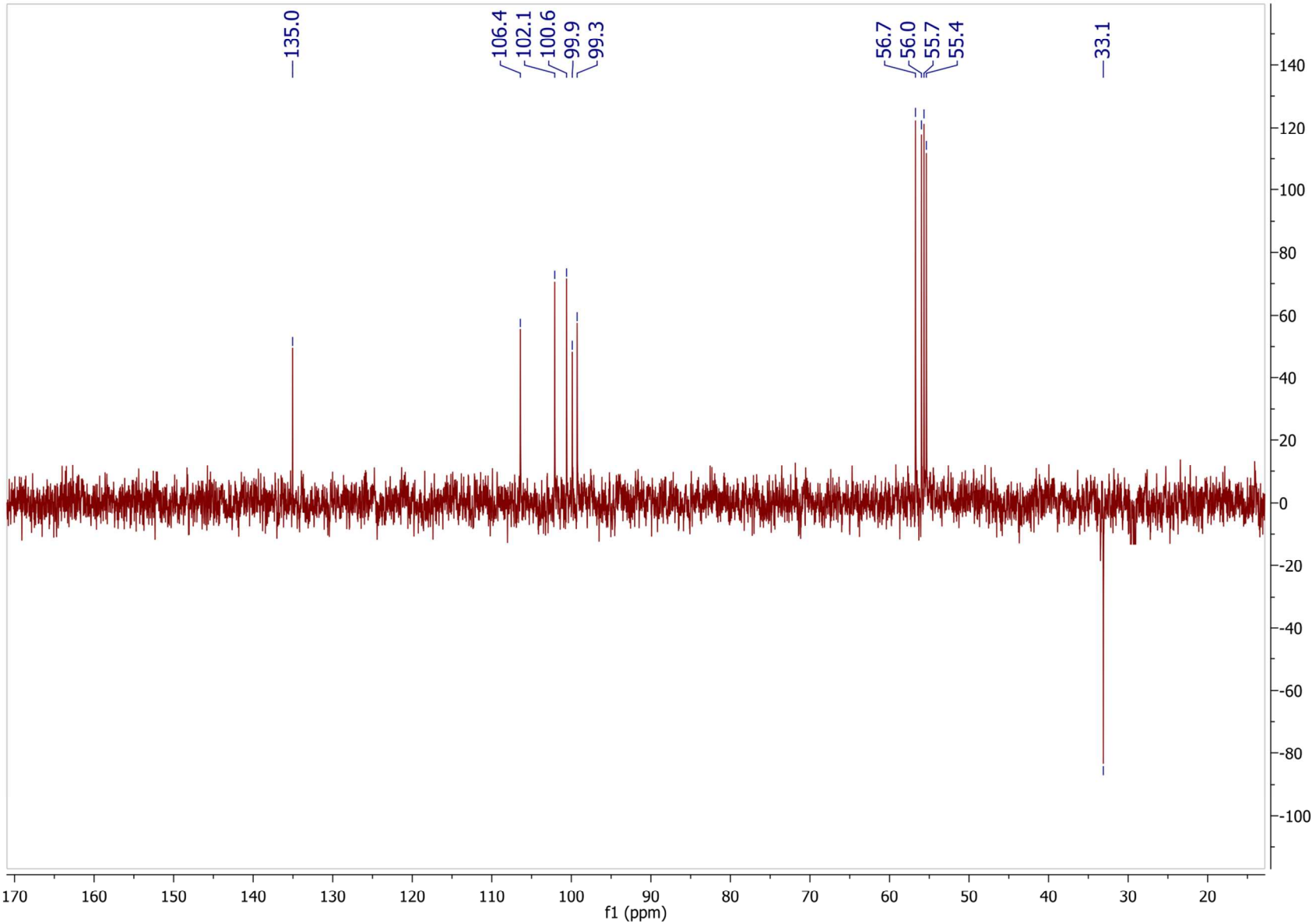

Figure S10. DEPT-135 spectrum of minimoidione B (**2**) in $CDCl_3$.

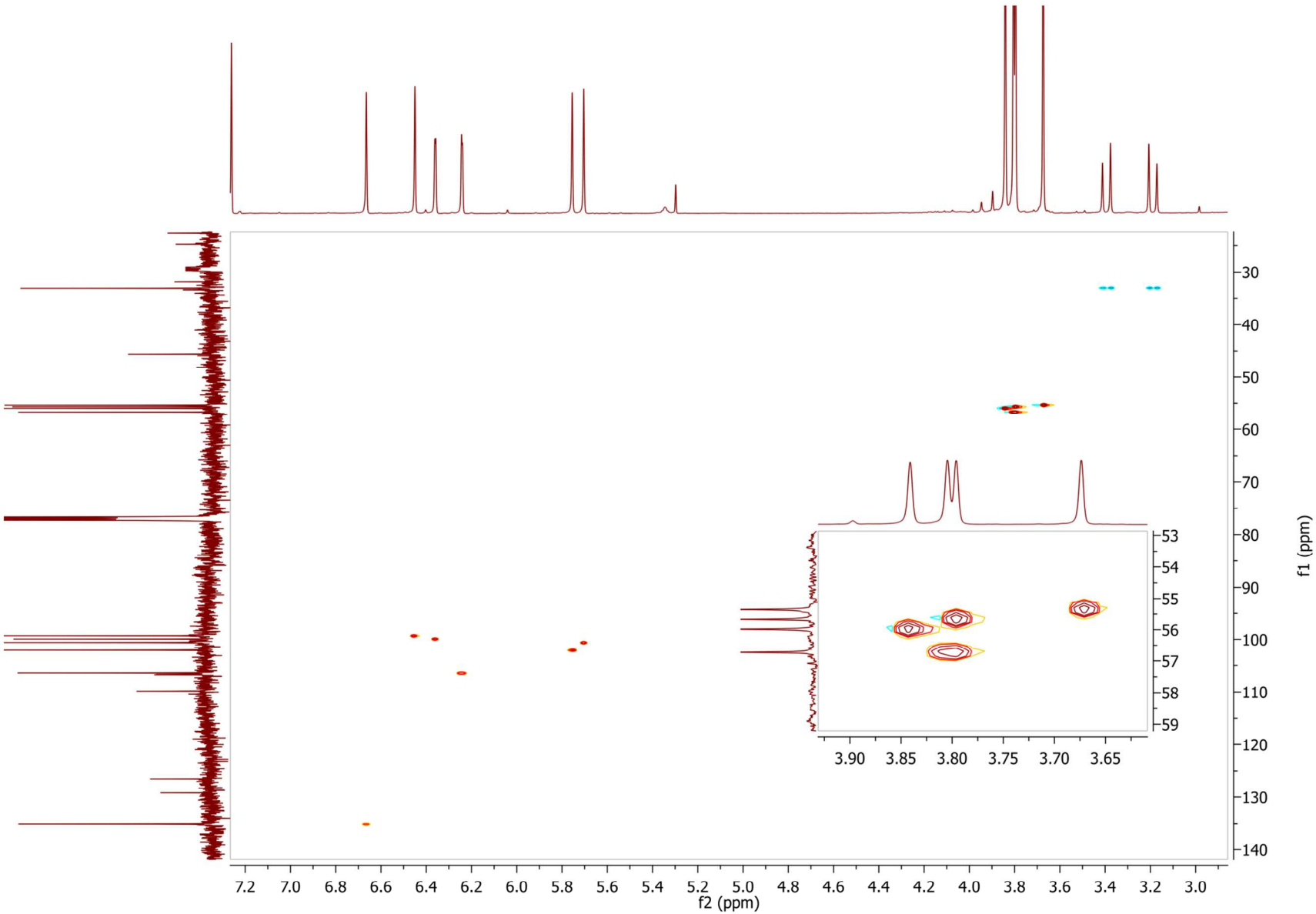

Figure S11. HSQC spectrum of minimoidione B (**2**) in $CDCl_3$.

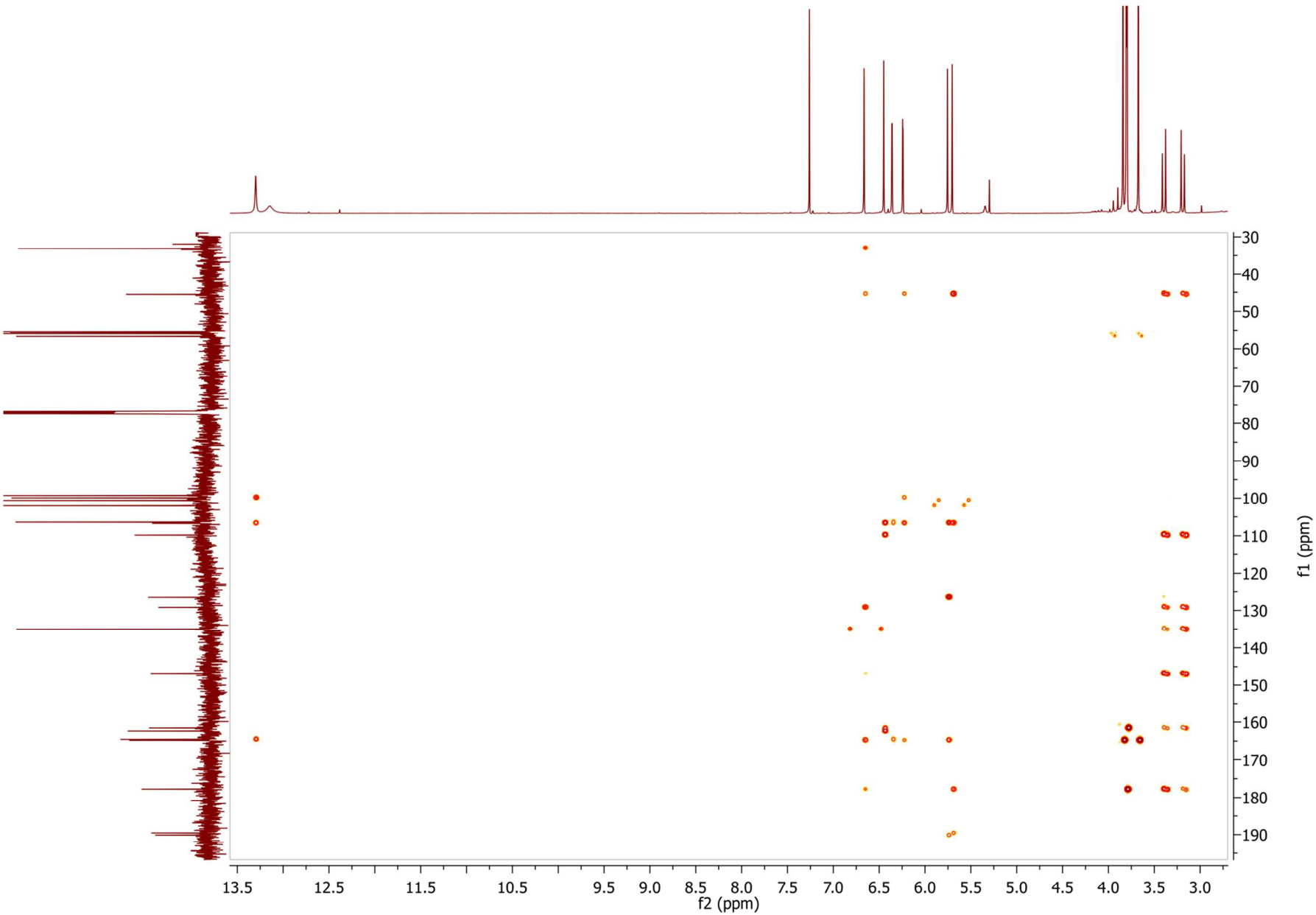

Figure S12. HMBC spectrum of minimoidione B (**2**) in $CDCl_3$.

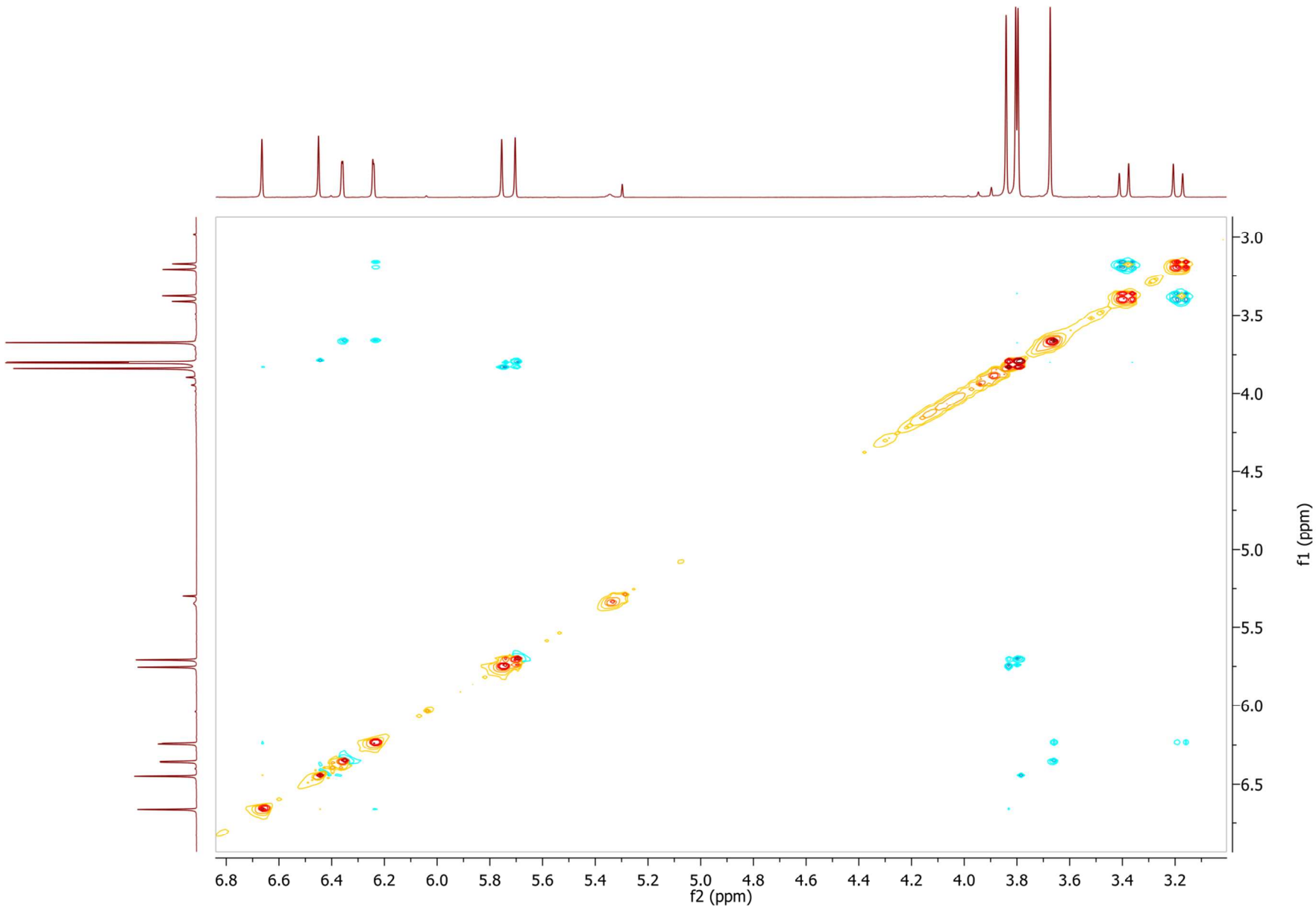

Figure S13. NOESY spectrum of minimoidione B (**2**) in $CDCl_3$.

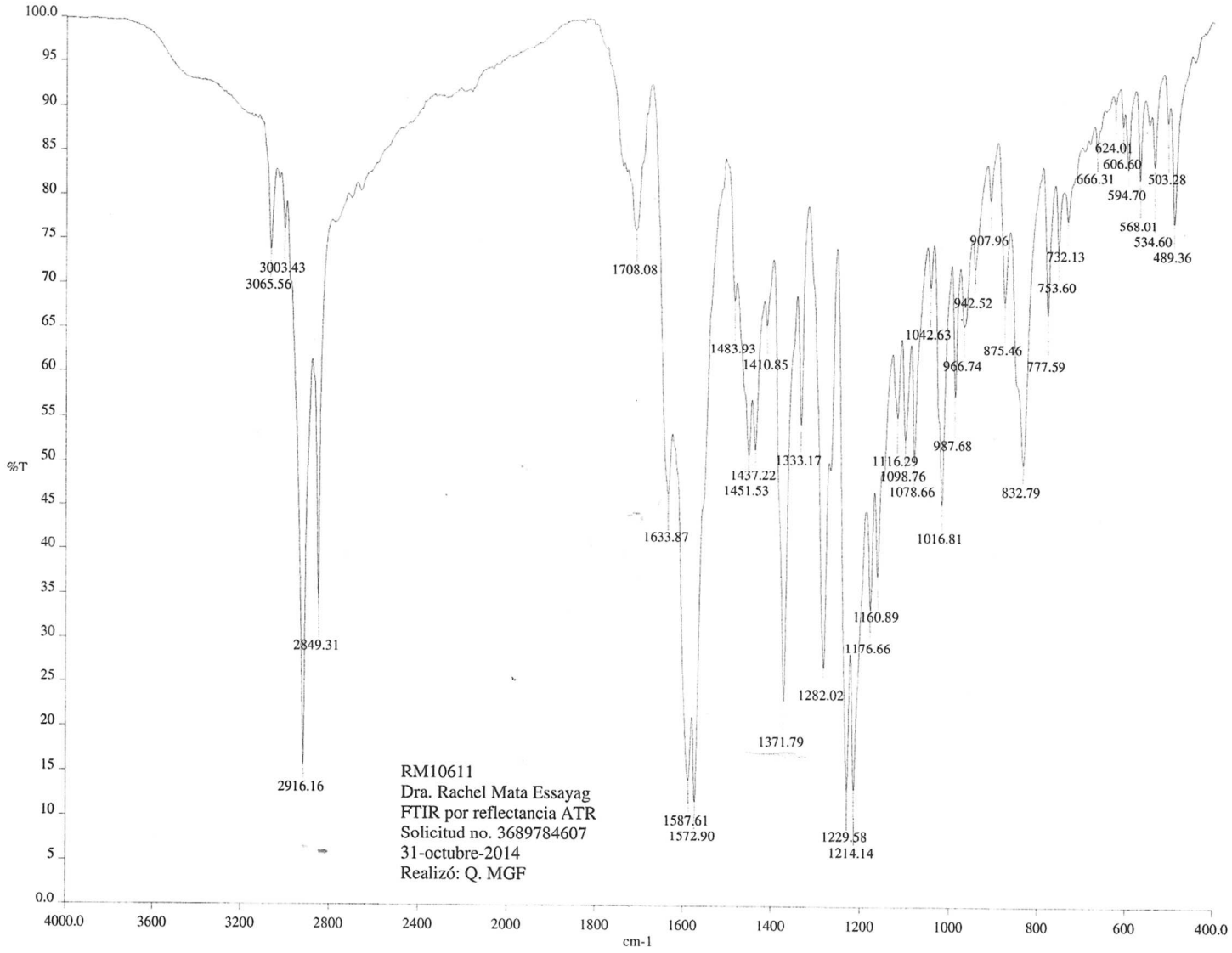

Figure S14. FTIR spectrum of minimoidione B (**2**).

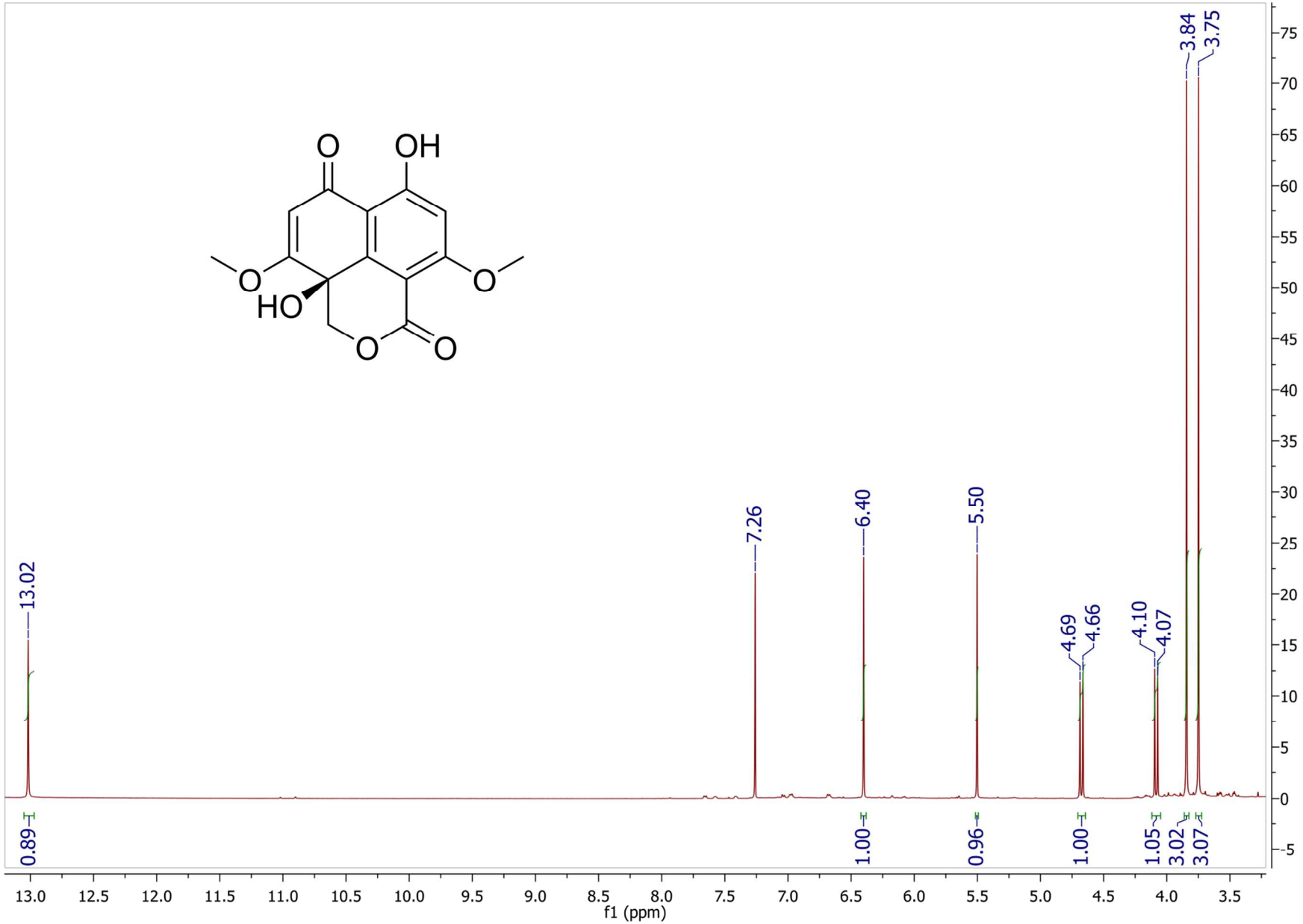

Figure S15. ^{1}H NMR spectrum of preussochromone C (**3**) in $CDCl_3$.

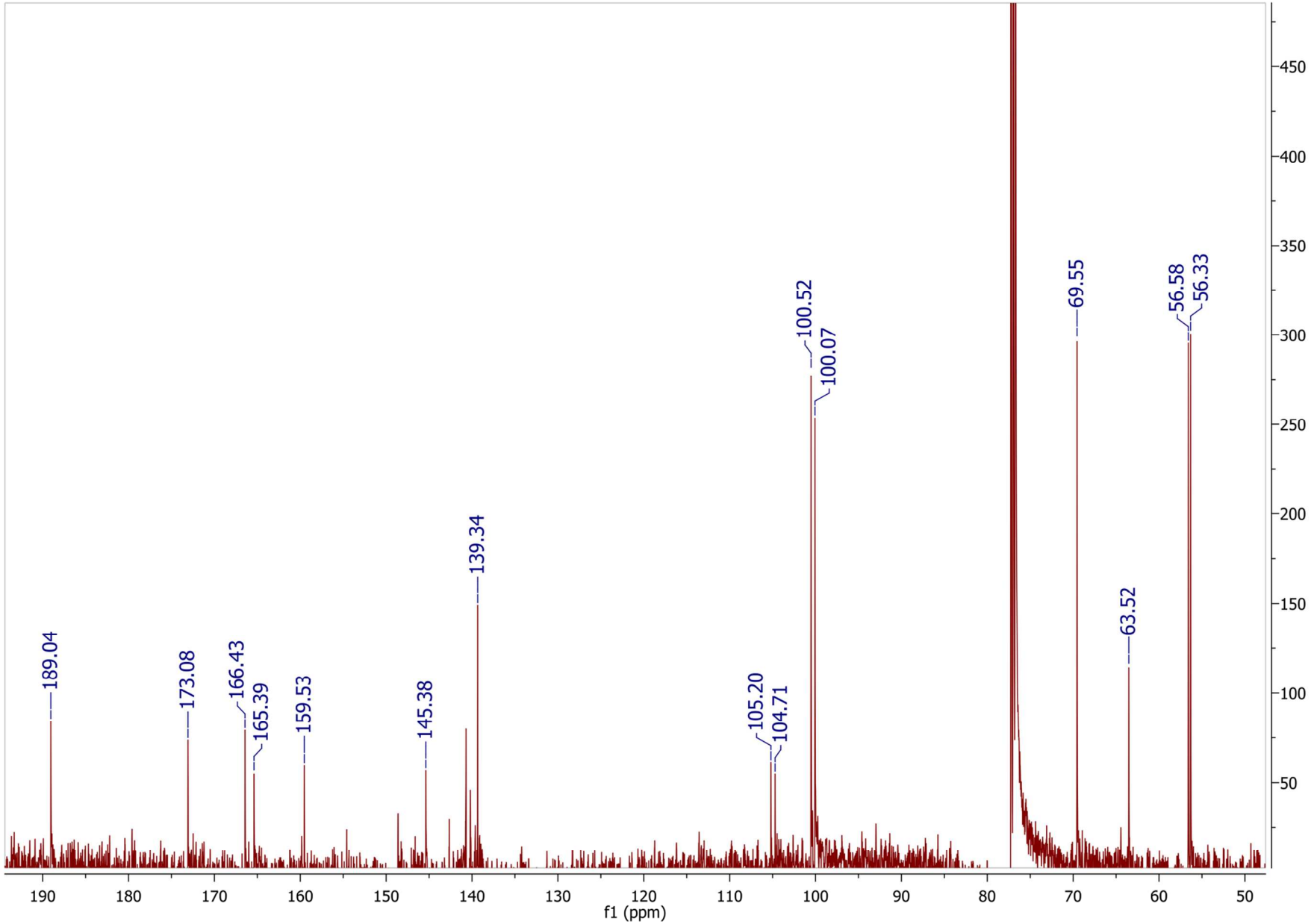

Figure S16. ^{13}C NMR spectrum of preussochromone C (**3**) in $CDCl_3$.

Figure S17. ^{1}H NMR spectrum of corymbiferone (**4**) in $CDCl_3$.

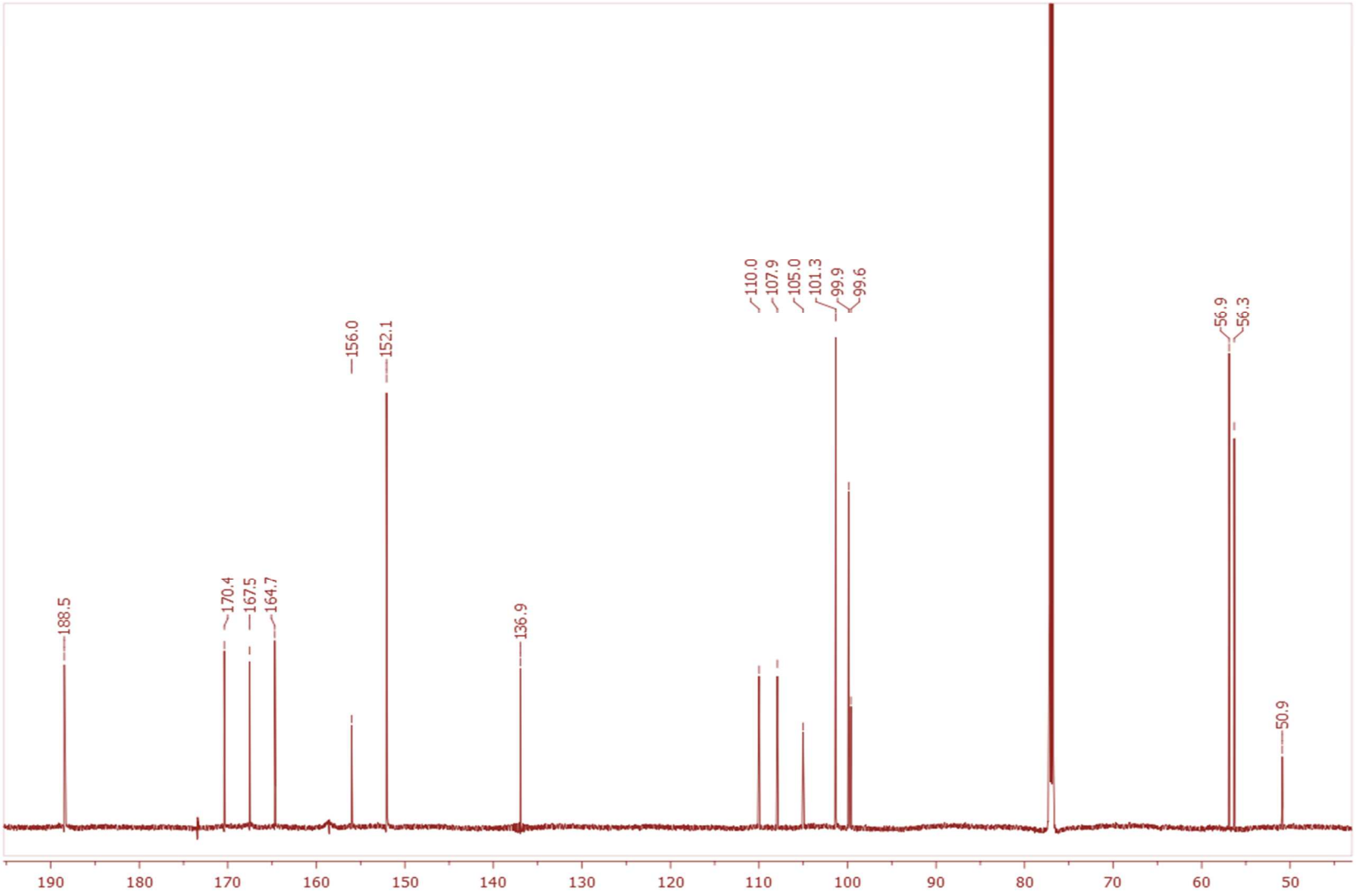

Figure S18. ^{13}C NMR spectrum of corymbiferone (**4**) in $CDCl_3$.

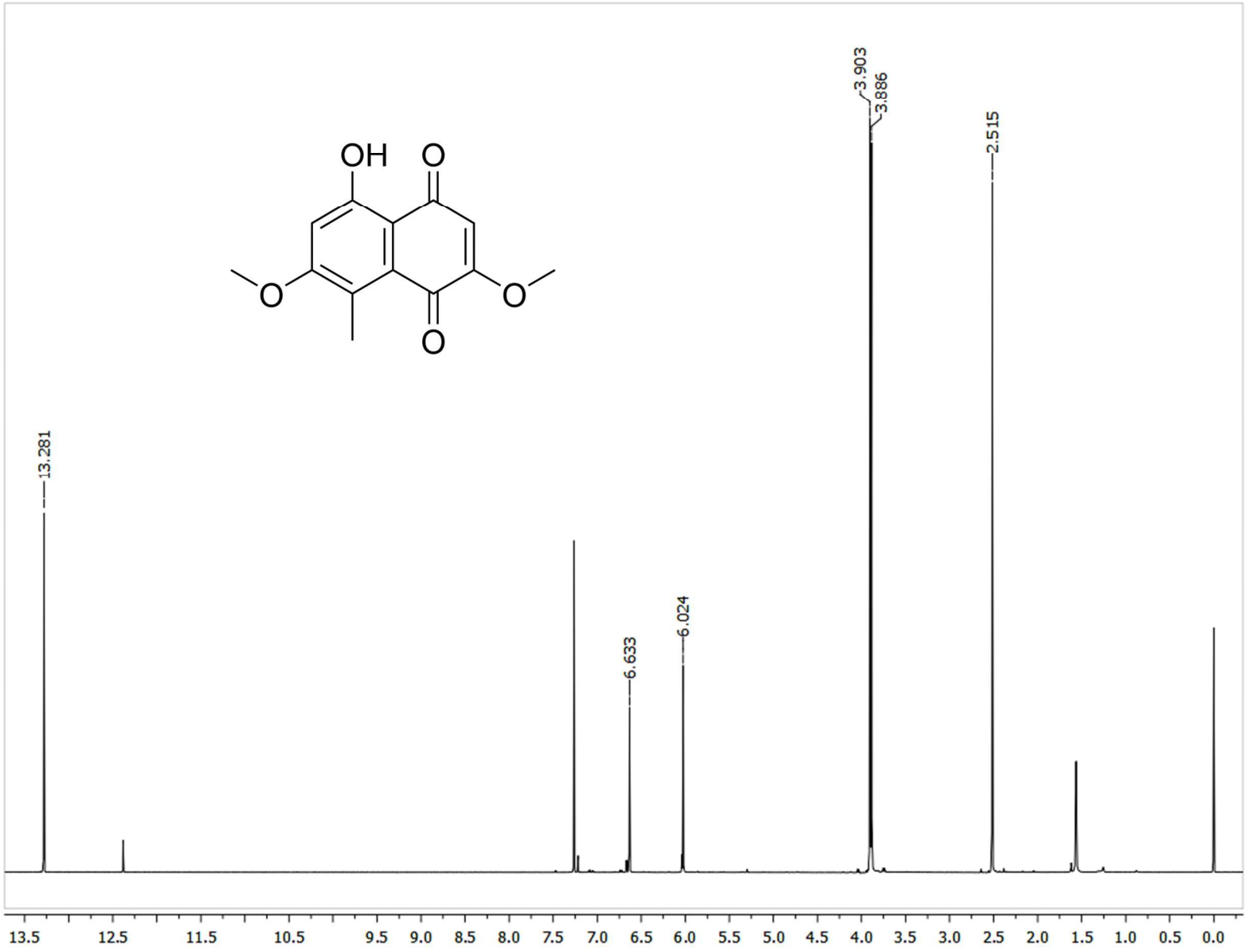

Figure S19. ^{1}H NMR spectrum of 5-hydroxy-2,7-dimethoxy-8-methylnaphthoquinone (**5**) in $CDCl_3$.

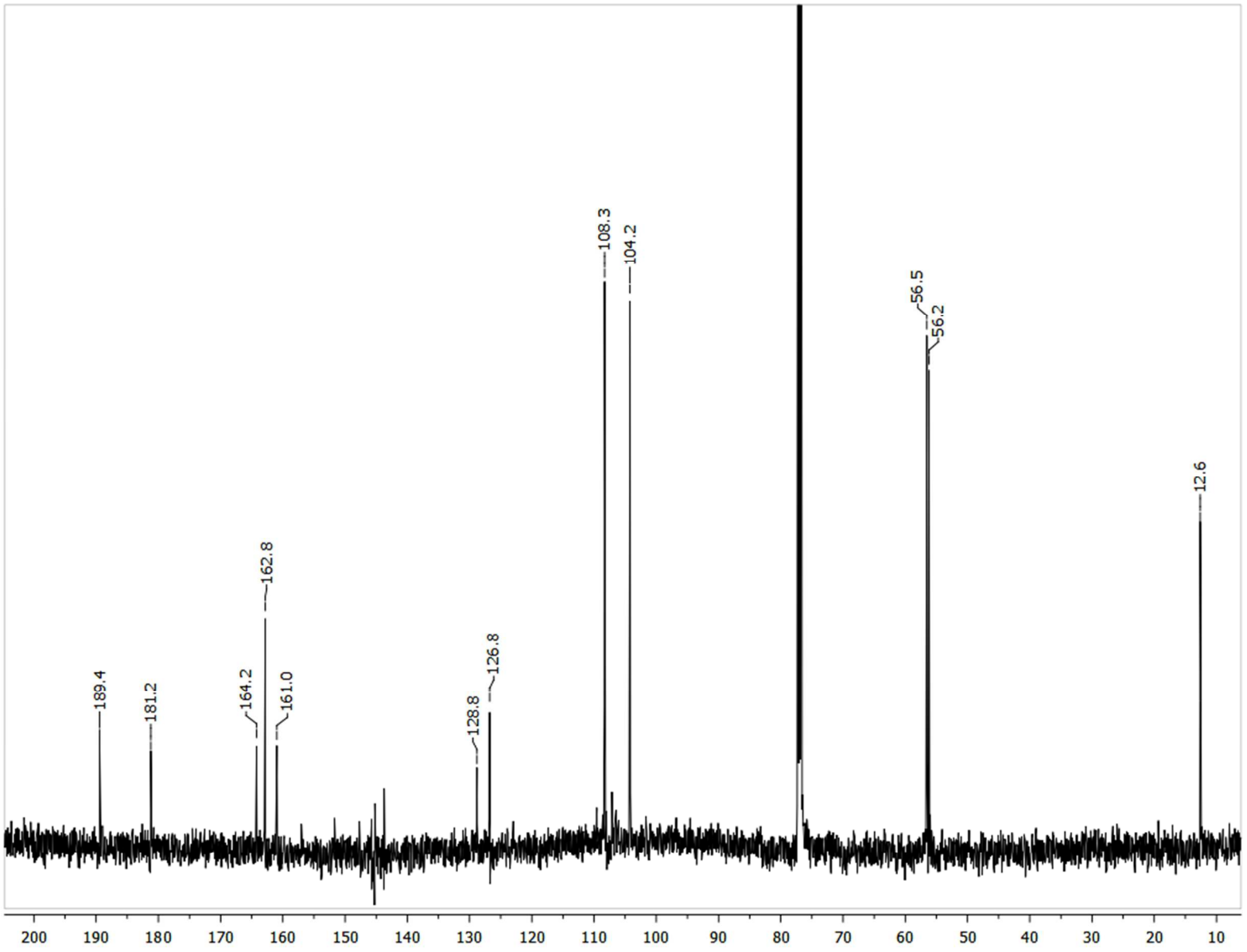

Figure S20. ^{13}C-NMR spectrum of 5-hydroxy-2,7-dimethoxy-8-methylnaphthoquinone (**5**) in $CDCl_3$.

Preussochromone C (3): yellow powder; mp: 243-245 °C; $[\alpha]^{25}_{D}$ +151 (1 mg/mL, MeOH); DC (*c* 0.01 mg/mL, $CHCl_3$) λ_{max} ($\Delta\varepsilon$) 336 (+2.1), 296 (-0.1), 255 (+6.9); ^{1}H-RMN (500 MHz, $CDCl_3$) δ_H (ppm): 13.15 (1H, s, OH-1), 6.53 (1H, s, H-2), 5.63 (1H, s, H-7), 4.81 (1H, d, *J* = 12 Hz, CH_2-10a), 4.21 (1H, d, *J* = 12 Hz, CH_2-10b), 3.97 (3H, s, CH_3O-12), 3.88 (3H, s, CH_3O-11); ^{13}C-RMN (175 MHz, $CDCl_3$) δ_C (ppm): 189.1 (C-8), 173.1 (C-6), 166.4 (C-1), 165.4 (C-3), 159.5 (C-9), 145.4 (C-4a), 105.2 (C-8a), 104.7 (C-4), 100.5 (C-7), 100.1 (C-2), 69.5 (C-10), 63.5 (C-5), 56.6 (CH_3O-12), 56.3 (CH_3O-11); ESIMS *m*/*z* 293 $[M+H]^+$.

Corymbiferone (4): yellow powder; mp: 255-257 °C; UV (MeOH) λ_{max}: 212, 245, 276, 364 nm; IR (FTIR-ATR) ν_{max}: 3474, 3074, 2949, 1741, 1647, 1588, 1561, 1381 cm^{-1}; ^{1}H-RMN (700 MHz, $CDCl_3$) δ_H (ppm): 14.56 (1H, s, OH-8), 8.25 (1H, s, H-10), 6.57 (1H, s, H-7), 5.92 (1H, s, H-2), 4.06 (3H, s, CH_3O-6), 3.96 (3H, s, CH_3O-3); ^{13}C-RMN (175 MHz, $CDCl_3$) δ_C (ppm): 188.5 (C-1), 170.4 (C-8), 167.5 (C-6), 165.0 (C-3), 156.0 (C-9), 152.1 (C-10), 136.9 (C-4a), 107.9 (C-4), 105.0 (C-8a), 101.3 (C-2), 99.9 (C-7), 99.6 (C-5), 56.9 (CH_3O-6), 56.3 (CH_3O-3); ESIMS *m*/*z* 275 $[M+H]^+$.

5-Hydroxy-2,7-dimethoxy-8-methylnaphthoquinone (5): orange powder; mp: 165–167 °C; UV (MeOH) λ_{max} (log ε): 220 (4.5), 265 (4.1), 297 (4.0) nm; IR (FTIR-ATR) ν_{max}: 3067, 2929, 1678, 1632, 1600, 1434, 1373, 1237 cm^{-1}; ^{1}H-RMN (500 MHz, $CDCl_3$) δ_H (ppm): 13.28 (1H, s, OH-5), 6.63 (1H, s, H-6), 6.02 (1H, s, H-3), 3.90 (3H, s, CH_3O-7), 3.88 (3H, s, CH_3O-2), 2.52 (3H, s, CH_3-8); ^{13}C-RMN (125 MHz, $CDCl_3$) δ_C (ppm): 189.4 (C, C-4), 181.2 (C, C-1), 164.2 (C, C-7), 162.8 (C, C-5), 161.0 (C, C-2), 128.8 (C, C-8a), 126.8 (C, C-8), 108.4 (C, C-5a), 108.3 (CH, C-3), 104.2 (CH, C-6), 56.5 (CH_3, OCH_3-2), 56.2 (CH_3, OCH_3-7), 12.6 (CH_3, C-8); HRESIMS *m*/*z* 249.0680 $[M+H]^+$ (calcd for $C_{13}H_{12}O_5$, 248.0684).

Table S1. Geometry Optimization and ^{1}H NMR Single-Point Calculations at DFT B3LYP/6-311+G(2d,p) Level of Theory for Minimoidione A (**1**).

Conformer	Gauss Energy	Energy (kcal/mol)	ΔG	Molar Fraction (kcal/mol)
01	-1338.917	-840183.58306	0.00000	0.499892
02	-1338.917	-840183.58306	0.00000	0.499892
04	-1338.91	-840178.58181	5.00125	1.08E-04
03	-1338.91	-840178.58055	5.00251	1.08E-04

Conformer				Calculated chemical shift (δ)						
01	02	03	04	δ_{01}	δ_{02}	δ_{03}	δ_{04}	δ_{calcd}*	δ_{exp}	$\lvert\delta_{exp}-\delta_{calcd}\rvert$
25.4184	25.4184	25.3457	25.3457	6.18624696	6.18624696	6.25435638	6.25435638	6.19	6.49	0.3037
26.234	26.234	25.6745	25.6746	5.42214727	5.42214727	5.94631816	5.94622447	5.42	5.65	0.2277
24.4064	24.4064	24.5921	24.5919	7.13434514	7.13434514	6.96037099	6.96055837	7.13	6.98	0.1543
27.491	27.491	27.4635	27.4634	4.24451939	4.24451939	4.27028293	4.27037662	4.24	4.28	0.0355
30.8896	30.8896	30.9113	30.9113	1.06052089	1.06052089	1.04019112	1.04019112	1.06	1.28	0.2195
30.8592	30.8591	30.9582	30.9581	1.08900131	1.089095	0.99625258	0.99634626	1.09	1.28	0.1910
30.3637	30.3637	30.3591	30.359	1.55321342	1.55321342	1.55752295	1.55761664	1.55	1.28	0.2732
27.481	27.481	27.4467	27.4466	4.25388795	4.25388795	4.28602211	4.2861158	4.25	4.25	0.0039
26.3332	26.3332	26.2392	26.2392	5.32921117	5.32921117	5.41727562	5.41727562	5.33	5.5	0.1708
27.9543	27.9543	27.9509	27.9508	3.81047405	3.81047405	3.81365936	3.81375304	3.81	5.30	1.4895
18.1785	18.1784	18.3402	18.3399	12.9689901	12.9690838	12.8175005	12.8177815	12.97	13.21	0.2410
28.1613	28.1613	28.2214	28.2217	3.61654488	3.61654488	3.56023984	3.55995878	3.62	3.80	0.1835
27.802	27.802	27.7555	27.7554	3.9531572	3.9531572	3.996721	3.99681469	3.95	3.80	0.1532
28.1716	28.1716	28.4389	28.4389	3.60689526	3.60689526	3.35647367	3.35647367	3.61	3.80	0.1932
28.0393	28.0718	28.0474	28.0478	3.7308413	3.70039348	3.72325276	3.72287802	3.72	3.90	0.1844
28.0718	27.7726	28.1222	28.122	3.70039348	3.98070077	3.65317594	3.65336331	3.84	3.90	0.0595
27.7726	28.0393	27.6663	27.6663	3.98070077	3.7308413	4.08028855	4.08028855	3.86	3.90	0.0442
28.1307	28.5082	28.1098	28.5549	3.64521267	3.29154956	3.66479295	3.24779839	3.47	3.53	0.0616
28.505	28.1307	28.4957	28.1099	3.2945475	3.64521267	3.30326026	3.66469927	3.47	3.53	0.0601
28.5082	28.505	28.5549	28.4957	3.29154956	3.2945475	3.24779839	3.30326026	3.29	3.53	0.2370

*Computed with B3LYP/6-311+G(2d,p)//B3LYP/6-311+G(2d,p).

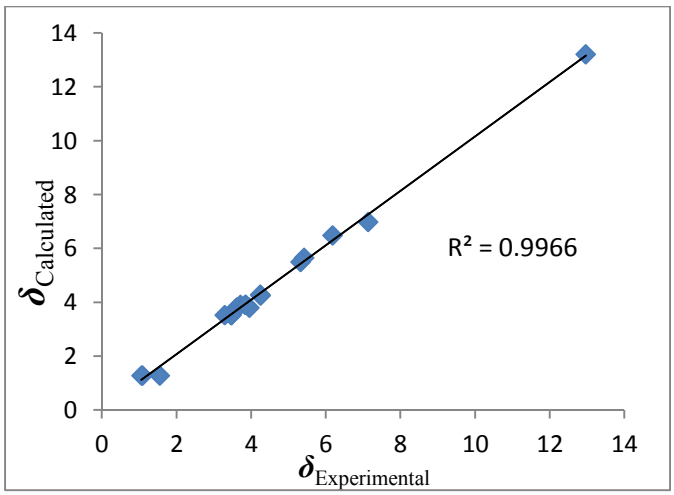

$$\mathrm{MAE} = |\Delta\delta_{\mathrm{ave}}| = \frac{1}{N}\sum_{i=1}^{N}\left|\delta_i^{\mathrm{comp}} - \delta_i^{\mathrm{exp}}\right|$$

Mean absolute error (MAE): 0.158

Table S2. Comparison of Computed and Experimental ^{1}H NMR Data for **1**.

Position	$\delta_{\mathrm{H\ Exp}}$	$\delta_{\mathrm{H\ Calcd}}$*
2	6.49	6.19
5	5.65	5.42
7	6.98	7.13
8	4.25	4.25
10	5.50	5.33
11a	4.28	4.24
1-OCH_3	3.90	3.87
6-OCH_3	3.80	3.72
11-OCH_3	3.53	3.41
7a-CH_3	1.28	1.23
3-OH	13.21	12.97
MAE	0.158	

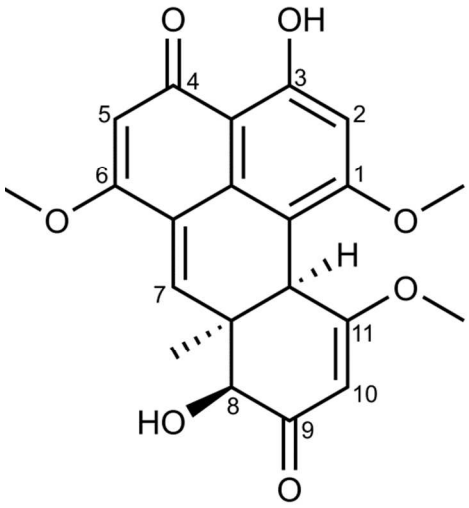

*Chemical shifts were derived from application of scaling factors (slope = −1.0674, intercept = 32.0216) to the ^{1}H NMR shielding tensors computed at the B3LYP/6-311+G(2d,p) level of theory.

Table S3. Calculated DFT B3LYP/6-31+G(d) Free Energies, Population and Theoretical Averaged Rotatory Strength Values Expressed in *R(len)* for Conformers of 7a*S*,8*S*,11a*S* Enantiomer of **1.**

		Conformer					
		1	2	3	4		
	ΔG^a	0	0	4.743	4.741	Weighted valued[d]	λ(nm)[e]
	P(%)[b]	49.98	49.98	0.02	0.02		
	1	-5.711	-5.711	0.071	1.01	-5.709	415.564
	2	13.707	13.707	40.183	59.118	13.72	352.95
	3	-0.917	-0.917	-26.022	-41.551	-0.929	330.375
	4	-3.205	-3.204	1.58	0.993	-3.203	329.18
	5	2.871	2.871	-0.439	-0.363	2.87	318.324
	6	-31.171	-31.173	-45.596	-1.429	-31.169	300.221
	7	40.434	40.435	52.548	-15.149	40.426	292.981
	8	4.608	4.608	10.126	26.242	4.612	284.751
	9	-2.952	-2.952	-1.86	-2.16	-2.951	280.661
	10	10.116	10.116	-7.219	-2.32	10.11	267.994
	11	-45.18	-45.179	8.044	-4.275	-45.162	262.462
	12	7.836	7.835	-14.377	9.083	7.832	258.211
	13	22.316	22.317	-6.076	-4.665	22.306	256.3
	14	-15.158	-15.158	-29.079	-5.416	-15.159	252.68
	15	72.34	72.338	13.482	3.818	72.316	246.511
n-states[c]	16	26.981	26.983	92.552	-5.54	26.988	232.845
	17	-65.025	-65.027	-27.92	1.21	-65.007	231.851
	18	19.253	19.253	-9.582	77.071	19.259	229.23
	19	33.936	33.935	2.836	-1.8	33.923	226.67
	20	-28.349	-28.339	-7.36	-5.988	-28.336	224.53
	21	-15.015	-15.026	85.198	5.479	-14.999	224.119
	22	-1.86	-1.859	3.204	0.42	-1.858	221.339
	23	33.986	33.986	-18.418	-0.485	33.97	219.809
	24	-23.998	-24	5.157	-10.902	-23.991	216.28
	25	-42.527	-42.523	-83.157	-59.659	-42.535	214.97
	26	-10.63	-10.629	-0.483	-10.505	-10.628	214.539
	27	-2.357	-2.358	-10.299	-12.206	-2.361	211.6
	28	17.316	17.308	1.833	27.959	17.311	209.569
	29	-23.766	-23.758	-8.522	-1.45	-23.755	209.289
	30	-6.661	-6.662	2.304	0.439	-6.658	206.99

[a]DFT B3LYP/6-31+G(d) Gibbs free energies in kcal mol^{-1} relative to the absolute G value for the global minimum –840032.1537 kcal mol^{-1}. [b]In percent from ΔG values at 298 K and 1 atm. [c]DFT B3LYP/6-31+G(d) Rotatory strength values expressed in *R*(*len*). [d]Calculated with the equation $\Sigma iR(len)i \times Pi$, where *R*(*len*)*i* is the theoretical *R*(*len*) value calculated for the *n* = 1-30 excitation state and *Pi* is the population for the i^{th} conformer. [e]Averaged excitation state.

Table S4. Calculated DFT B3LYP/6-31+G(d) Free Energies, Population and Theoretical Averaged Rotatory Strength Values Expressed in $R_{(len)}$ for Conformers of 7a*R*,8*R*,11a*R* Enantiomer of **1.**

		Conformer					
		1	2	3	4		
	ΔG^a	0	0	4.743	4.741	Weighted valued[d]	λ(nm)[e]
	P(%)[b]	49.98	49.98	0.02	0.02		
	1	5.711	5.711	-0.071	-1.010	5.709	415.564
	2	-13.707	-13.707	-40.183	-59.118	-13.720	352.95
	3	0.917	0.917	26.022	41.551	0.929	330.375
	4	3.205	3.204	-1.580	-0.993	3.203	329.18
	5	-2.871	-2.871	0.439	0.363	-2.870	318.324
	6	31.171	31.173	45.596	1.429	31.169	300.221
	7	-40.434	-40.435	-52.548	15.149	-40.426	292.981
	8	-4.608	-4.608	-10.126	-26.242	-4.612	284.751
	9	2.952	2.952	1.860	2.160	2.951	280.661
	10	-10.116	-10.116	7.219	2.320	-10.110	267.994
	11	45.180	45.179	-8.044	4.275	45.162	262.462
	12	-7.836	-7.835	14.377	-9.083	-7.832	258.211
	13	-22.316	-22.317	6.076	4.665	-22.306	256.3
	14	15.158	15.158	29.079	5.416	15.159	252.68
	15	-72.340	-72.338	-13.482	-3.818	-72.316	246.511
n-states[c]	16	-26.981	-26.983	-92.552	5.540	-26.988	232.845
	17	65.025	65.027	27.920	-1.210	65.007	231.851
	18	-19.253	-19.253	9.582	-77.071	-19.259	229.23
	19	-33.936	-33.935	-2.836	1.800	-33.923	226.67
	20	28.349	28.339	7.360	5.988	28.336	224.53
	21	15.015	15.026	-85.198	-5.479	14.999	224.119
	22	1.860	1.859	-3.204	-0.420	1.858	221.339
	23	-33.986	-33.986	18.418	0.485	-33.970	219.809
	24	23.998	24.000	-5.157	10.902	23.991	216.28
	25	42.527	42.523	83.157	59.659	42.535	214.97
	26	10.630	10.629	0.483	10.505	10.628	214.539
	27	2.357	2.358	10.299	12.206	2.361	211.6
	28	-17.316	-17.308	-1.833	-27.959	-17.311	209.569
	29	23.766	23.758	8.522	1.450	23.755	209.289
	30	6.661	6.662	-2.304	-0.439	6.658	206.99

[a]DFT B3LYP/6-31+G(d) Gibbs free energies in kcal mol^{-1} relative to the absolute G value for the global minimum –840032.1537 kcal mol^{-1}. [b]In percent from ΔG values at 298 K and 1 atm. [c]DFT B3LYP/6-31+G(d) Rotatory strength values expressed in $R(len)$. [d]Calculated with the equation $\Sigma iR(len)i \times Pi$, where $R(len)i$ is the theoretical $R(len)$ value calculated for the n = 1-30 excitation state and Pi is the population for the i^{th} conformer. [e]Averaged excitation state.

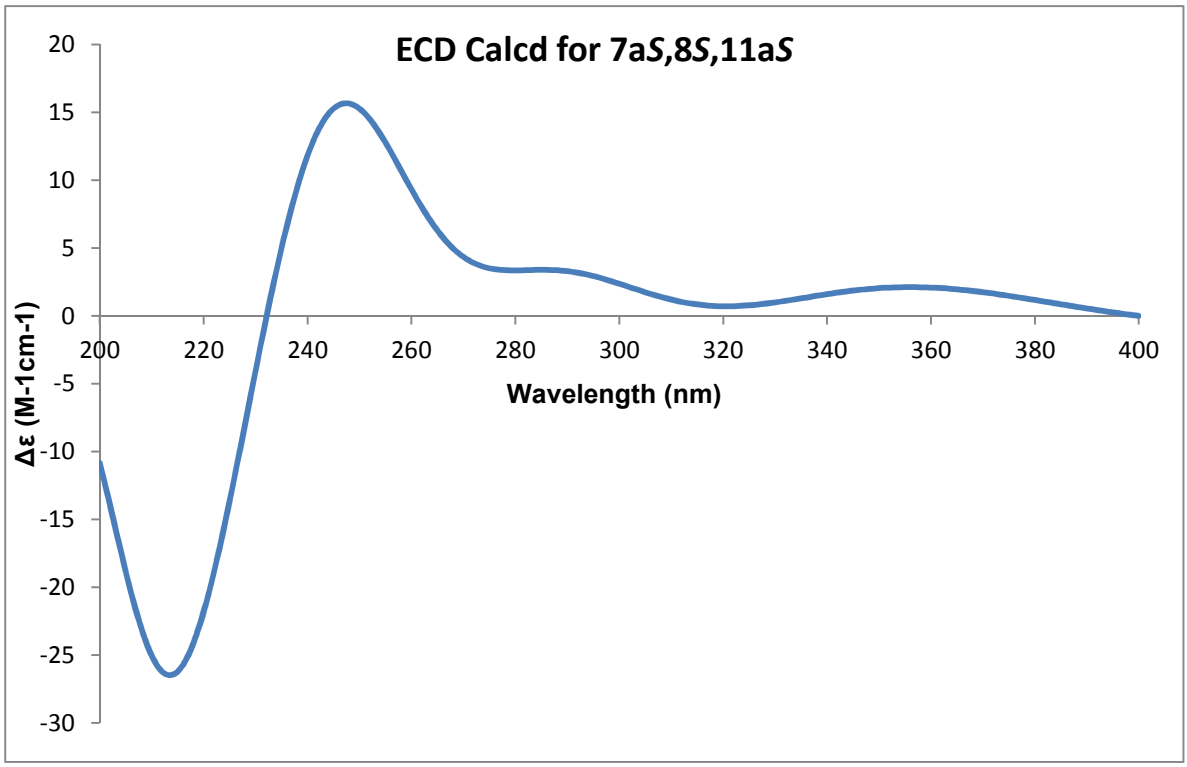

Figure S21. Calculated ECD at DFT B3LYP/6-31+G(d) theory Level for 7a*S*,8*S*,11a*S* enantiomer of **1**.

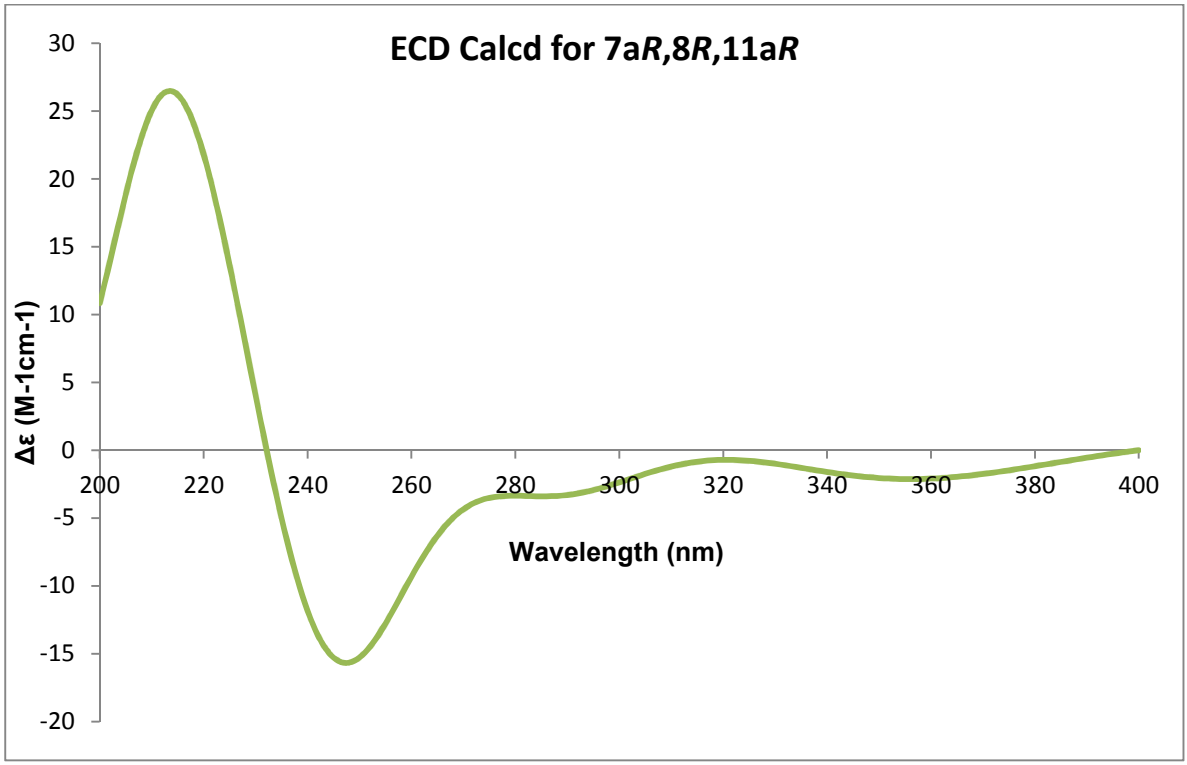

Figure S22. Calculated ECD at DFT B3LYP/6-31+G(d) theory Level for 7a*R*,8*R*,11a*R* enantiomer of **1**.

Table S5. Geometry Optimization and ^{1}H NMR Single-Point Calculations at DFT B3LYP/6-311+G(2d,p) Level of Theory for *R* Enantiomer of Minimoidione B (**2**).

Conformers	Gauss Energy	Energy (kcal/mol)	ΔG	Molar Fraction (kcal/mol)
1	-1605.912417	-1007725.47	0.00	0.3679715
2	-1605.912298	-1007725.40	0.07	0.2979745
4	-1605.911725	-1007725.04	0.43	0.1758294
3	-1605.911618	-1007724.97	0.50	0.1582246

Conformer				Calculated chemical shift (δ)						
01	02	03	04	δ_{01}	δ_{02}	δ_{03}	δ_{04}	δ_{calcd}*	δ_{exp}	$\lvert\delta_{exp}-\delta_{calcd}\rvert$
25.3947	25.5191	25.3794	25.2929	6.20845044	6.09190556	6.22278434	6.30382237	6.19	6.36	0.1641
25.3519	25.7241	25.6406	25.4295	6.24854787	5.8998501	5.97807757	6.17584785	6.09	6.24	0.1537
26.3886	26.0781	25.9862	26.389	5.27730935	5.56820311	5.65430017	5.27693461	5.42	5.70	0.2792
28.7284	28.7656	28.7277	28.7055	3.08525389	3.05040285	3.08590969	3.10670789	3.08	3.19	0.1101
28.3736	28.6768	28.5449	28.3813	3.41765037	3.13359565	3.25716695	3.41043657	3.31	3.39	0.0875
25.134	24.7947	24.8138	25.1162	6.45268878	6.77056399	6.75267004	6.46936481	6.60	6.66	0.0659
26.1652	26.1359	26.0287	26.1343	5.48660296	5.51405284	5.61448379	5.51555181	5.52	5.75	0.2338
25.3816	25.4171	25.3712	25.3549	6.22072325	6.18746487	6.23046655	6.24573731	6.22	6.45	0.2321
17.9757	17.9201	18.3085	18.302	13.1589844	13.2110736	12.8471988	12.8532884	13.07	13.30	0.2272
28.0671	28.1252	28.179	28.0594	3.7047967	3.65036537	3.59996253	3.71201049	3.67	3.79	0.1216
28.0592	28.1645	28.2656	28.0511	3.71219786	3.61354694	3.5188308	3.7197864	3.65	3.79	0.1414
27.7667	27.8719	27.9628	27.7495	3.98622822	3.88767098	3.80251077	4.00234214	3.93	3.79	0.1357
27.8571	27.7599	27.7791	27.851	3.90153644	3.99259884	3.9746112	3.90725126	3.94	3.84	0.1013
28.2354	28.1669	28.1137	28.2188	3.54712385	3.61129848	3.66113922	3.56267566	3.59	3.84	0.2529
28.2343	28.2205	27.95	28.2187	3.54815439	3.56108301	3.81450253	3.56276935	3.60	3.84	0.2432
28.1235	28.3524	28.7544	28.2259	3.65195803	3.43751171	3.06089563	3.55602398	3.48	3.67	0.1949
28.1085	28.3526	28.5618	28.2609	3.66601087	3.43732434	3.24133408	3.52323403	3.51	3.67	0.1670
27.8766	28.0052	28.1685	27.9317	3.88326775	3.76278808	3.60979951	3.83164699	3.80	3.67	0.1224
28.3915	28.0663	28.1732	28.3765	3.40088064	3.70554619	3.60539629	3.41493348	3.53	3.80	0.2770
28.2079	27.7904	27.7235	28.1835	3.57288739	3.96402473	4.02670039	3.59574667	3.77	3.80	0.0382
28.4171	28.1349	28.2778	28.3821	3.37689713	3.64127787	3.50740116	3.40968709	3.48	3.80	0.3214
18.2267	18.1742	18.1985	18.1953	12.9238336	12.9730185	12.950253	12.9532509	12.95	13.14	0.1954

*Computed with B3LYP/6-311+G(2d,p)//B3LYP/6-311+G(2d,p).

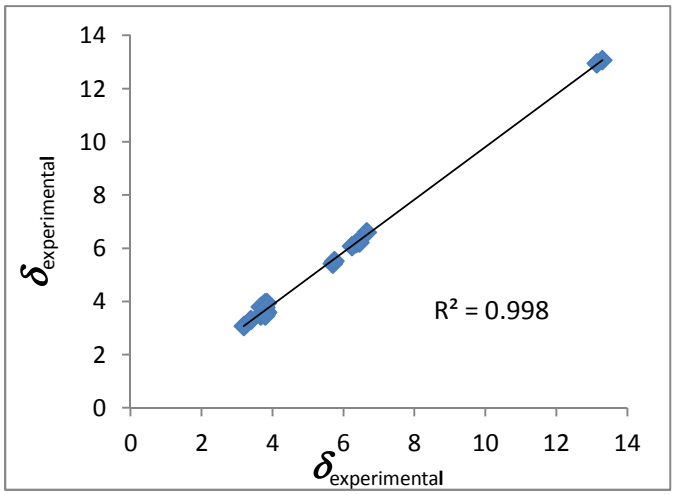

$$\mathrm{MAE} = |\Delta\delta_{\mathrm{ave}}| = \frac{1}{N}\sum_{i=1}^{N}\left|\delta_i^{\mathrm{comp}} - \delta_i^{\mathrm{exp}}\right|$$

Mean absolute error (MAE): 0.166

Table S6. Comparison of computed and experimental ^{1}H NMR data for *R* enantiomer of **2**.

Position	$\delta_{\mathrm{H\ Exp}}$	$\delta_{\mathrm{H\ Calcd}}$*
3	5.70	5.42
6	6.36	6.19
8	6.24	6.09
2-OCH_3	3.80	3.59
7-OCH_3	3.67	3.59
1'	3.19	3.08
	3.39	3.31
2'	6.66	6.60
5'	5.75	5.52
8'	6.45	6.22
4'-OCH_3	3.84	3.71
9'-OCH_3	3.79	3.75
OH-5	13.30	13.07
OH-7'	13.14	12.95
MAE	0.166	

*Chemical shifts were derived from application of scaling factors (slope = −1.0674, intercept = 32.0216) to the ^{1}H NMR shielding tensors computed at the B3LYP/6-311+G(2d,p) Level of theory.

Table S7. Geometry Optimization and ^{1}H NMR Single-Point Calculations at DFT B3LYP/6-311+G(2d,p) Level of Theory for *S* Enantiomer of Minimoidione B (**2**).

Conformer	Gauss Energy	Energy (kcal/mol)	ΔG	Molar Fraction (kcal/mol)
1	-1605.912417	-1007725.471	0.00	0.5
3	-1605.912417	-1007725.471	0.00	0.5
2	-1605.911725	-1007725.037	0.43	0

Conformer			Calculated chemical shift (δ)					
01	02	03	δ_{01}	δ_{02}	δ_{03}	δ_{calcd}*	δ_{exp}	$\lvert\delta_{exp}-\delta_{calcd}\rvert$
25.3816	25.3549	25.3816	6.22072325	6.24573731	6.22072325	6.22	6.45	0.2282
26.1652	26.1343	26.1653	5.48660296	5.51555181	5.48650927	5.49	5.75	0.2673
25.134	25.1162	25.134	6.45268878	6.46936481	6.45268878	6.45	6.66	0.2110
28.7284	28.7055	28.7284	3.08525389	3.10670789	3.08525389	3.09	3.19	0.1036
28.3736	28.3813	28.3736	3.41765037	3.41043657	3.41765037	3.42	3.39	0.0239
25.3519	25.4295	25.3519	6.24854787	6.17584785	6.24854787	6.25	6.24	0.0057
25.3947	25.293	25.3947	6.20845044	6.30372869	6.20845044	6.21	6.36	0.1484
26.3886	26.389	26.3886	5.27730935	5.27693461	5.27730935	5.28	5.70	0.4255
17.9758	18.302	17.9758	13.1588908	12.8532884	13.1588908	13.16	13.30	0.1397
18.2268	18.1954	18.2266	12.9237399	12.9531572	12.9239273	12.92	13.14	0.2194
28.0592	28.0511	28.0592	3.71219786	3.7197864	3.71219786	3.71	3.79	0.0827
28.0671	28.0594	28.0671	3.7047967	3.71201049	3.7047967	3.70	3.79	0.0901
27.7667	27.7495	27.7667	3.98622822	4.00234214	3.98622822	3.99	3.79	0.1913
28.2354	28.2188	28.2354	3.54712385	3.56267566	3.54712385	3.55	3.84	0.2928
27.8571	27.8511	27.8571	3.90153644	3.90715758	3.90153644	3.90	3.84	0.0616
28.2343	28.2188	28.2343	3.54815439	3.56267566	3.54815439	3.55	3.84	0.2917
28.3916	28.3765	28.3916	3.40078696	3.41493348	3.40078696	3.40	3.80	0.4027
28.4171	28.3821	28.4171	3.37689713	3.40968709	3.37689713	3.38	3.80	0.4266
28.2079	28.1835	28.2079	3.57288739	3.59574667	3.57288739	3.57	3.80	0.2306
27.8766	27.9316	27.8766	3.88326775	3.83174068	3.88326775	3.88	3.67	0.2107
28.1085	28.2608	28.1085	3.66601087	3.52332771	3.66601087	3.67	3.67	0.0066
28.1235	28.2259	28.1235	3.65195803	3.55602398	3.65195803	3.65	3.67	0.0206

*Computed with B3LYP/6-311+G(2d,p)//B3LYP/6-311+G(2d,p).

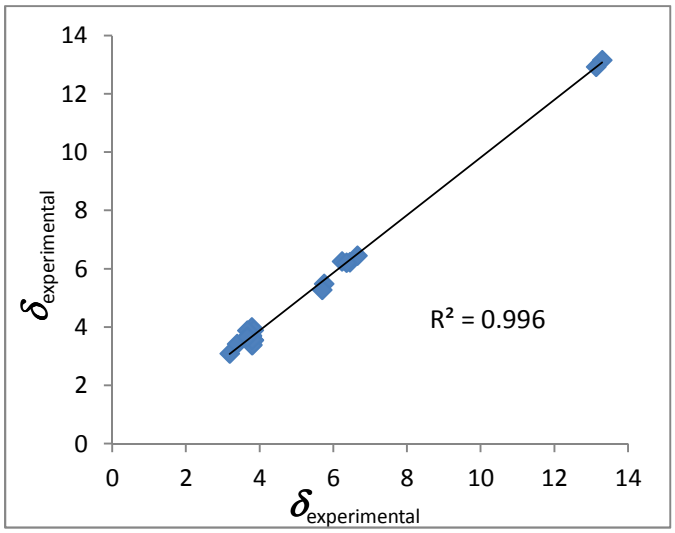

$$\mathrm{MAE} = |\Delta\delta_{\mathrm{ave}}| = \frac{1}{N}\sum_{i=1}^{N}\left|\delta_i^{\mathrm{comp}} - \delta_i^{\mathrm{exp}}\right|$$

Mean absolute error (MAE): 0.169

Table S8. Comparison of computed and experimental ^{1}H NMR data for *S* enantiomer of **2**.

Position	$\delta_{\mathrm{H\ Exp}}$	$\delta_{\mathrm{H\ Calcd}}$*
3	5.70	5.28
6	6.36	6.21
8	6.24	6.25
2-OCH_3	3.80	3.45
7-OCH_3	3.67	3.73
1'	3.19	3.09
	3.39	3.42
2'	6.66	6.45
5'	5.75	5.49
8'	6.45	6.22
4'-OCH_3	3.84	3.67
9'-OCH_3	3.79	3.80
OH-5	13.30	13.16
OH-7'	13.14	12.92
MAE	0.169	

*Chemical shifts were derived from application of scaling factors (slope = −1.0674, intercept = 32.0216) to the ^{1}H NMR shielding tensors computed at the B3LYP/6-311+G(2d,p) Level of theory.

Table S9. Inhibitory Effect and docking binding energies (Δ*G*) of Compounds **1**–**4** Tested Against Yeast α-Glucosidase (αGHY)

compound	**IC_{50} (μM)**	**Δ*G* (kcal mol^{-1})**
minimoidione A (**1**)	95.2 ± 0.8	−8.5
minimoidione B (**2**)	2.9 ± 0.47	−7.7 (*R*) −10.3 (*S*)
preussochromone C (**3**)	66.5 ± 0.97	−7.9
corymbiferone (**4**)	155.5 ± 4.25	−7.6
acarbose*	876.9 ± 38.8	−9.9

*Acarbose was used as positive control for αGHY.

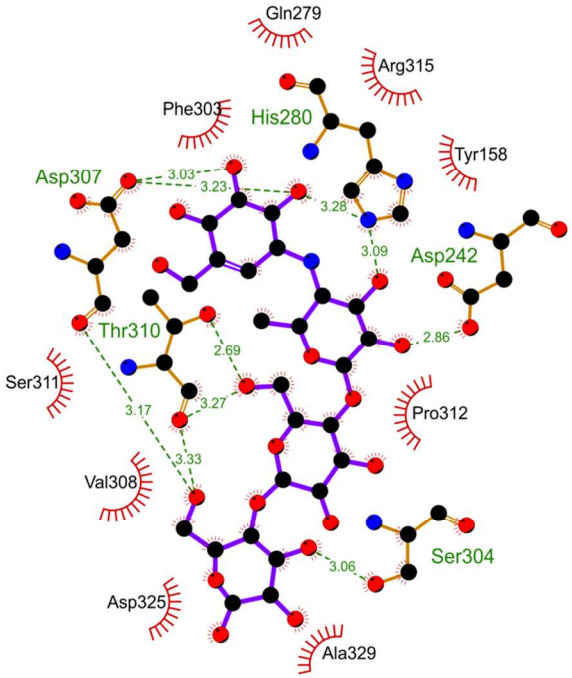

Figure S23. 2D Representation of the interactions among αGHY and acarbose in the predicted binding site.

Table S10. Crystal Data and Structure Refinement for Minimoidione A (**1**).

Identification code	072XYZ16	
Empirical formula	$C_{21}\ H_{20}\ O_7$	
Formula weight	384.37	
Temperature	150(2) K	
Wavelength	0.71073 Å	
Crystal system	Monoclinic	
Space group	P 2_1/n	
Unit cell dimensions	a = 9.1302(13) Å	α= 90°.
	b = 15.476(2) Å	β= 109.085(3)°.
	c = 13.420(2) Å	γ = 90°.
Volume	1792.0(4) Å^3	
Z	4	
Density (calculated)	1.425 Mg/m^3	
Absorption coefficient	0.107 mm^{-1}	
F(000)	808	
Crystal size	0.273 x 0.118 x 0.076 mm^3	
Theta range for data collection	2.382 to 25.193°.	
Index ranges	-10<=h<=10, -18<=k<=18, -16<=l<=15	
Reflections collected	10832	
Independent reflections	3193 [R(int) = 0.1193]	
Completeness to theta = 25.193°	99.0 %	
Refinement method	Full-matrix least-squares on F^2	
Data / restraints / parameters	3193 / 2 / 263	
Goodness-of-fit on F^2	0.970	
Final R indices [I>2sigma(I)]	R1 = 0.0568, wR2 = 0.1138	
R indices (all data)	R1 = 0.1021, wR2 = 0.1404	
Largest diff. peak and hole	0.354 and -0.426 e.Å^{-3}	

Atomic coordinates ($\times 10^4$) and equivalent isotropic displacement parameters ($Å^2 \times 10^3$) for preussiaminimoidione I (**1**). U(eq) is defined as one third of the trace of the orthogonalized U^{ij} tensor.

	x	y	z	U(eq)
O(1)	7495(2)	6098(1)	10434(1)	32(1)
O(2)	8813(2)	6064(1)	8998(2)	32(1)
O(3)	5736(2)	3495(1)	11525(1)	31(1)
O(4)	4343(2)	1091(1)	8919(2)	45(1)
O(5)	6836(2)	339(1)	10311(2)	47(1)
O(6)	10245(2)	2321(1)	9545(1)	27(1)
O(7)	9226(2)	3315(1)	7507(1)	27(1)
C(1)	7281(3)	5297(2)	10344(2)	24(1)
C(2)	6659(3)	4834(2)	11052(2)	25(1)
C(3)	6323(3)	3982(2)	10913(2)	23(1)
C(4)	6529(3)	3503(2)	10030(2)	22(1)
C(5)	5844(3)	2736(2)	9712(2)	26(1)
C(6)	5965(3)	2275(2)	8759(2)	26(1)
C(7)	7564(3)	2464(2)	8642(2)	22(1)
C(8)	7888(3)	3430(2)	8720(2)	21(1)
C(9)	8726(3)	3839(2)	8145(2)	21(1)
C(10)	9024(3)	4723(2)	8243(2)	23(1)
C(11)	8505(3)	5204(2)	8928(2)	22(1)
C(12)	7707(3)	4812(2)	9545(2)	21(1)
C(13)	7403(3)	3918(2)	9420(2)	20(1)
C(14)	5825(3)	1295(2)	8870(2)	30(1)
C(15)	7113(3)	928(2)	9780(2)	31(1)
C(16)	8634(3)	1272(2)	9969(2)	31(1)
C(17)	8860(3)	1974(2)	9447(2)	25(1)
C(18)	5482(3)	3904(2)	12418(2)	36(1)
C(19)	4662(3)	2584(2)	7775(2)	36(1)
C(20)	11615(3)	1905(2)	10227(2)	37(1)
C(21)	10226(3)	3676(2)	6986(2)	36(1)

Bond lengths [Å] and angles [°] for minimoidione A (**1**).

O(1)-C(1)	1.254(3)	C(7)-H(7)	1.0000
O(2)-C(11)	1.358(3)	C(8)-C(13)	1.385(3)
O(2)-H(2A)	0.859(10)	C(8)-C(9)	1.403(3)
O(3)-C(3)	1.349(3)	C(9)-C(10)	1.393(3)
O(3)-C(18)	1.439(3)	C(10)-C(11)	1.381(3)
O(4)-C(14)	1.412(3)	C(10)-H(10)	0.9500
O(4)-H(4)	0.860(10)	C(11)-C(12)	1.407(3)
O(5)-C(15)	1.233(3)	C(12)-C(13)	1.409(3)
O(6)-C(17)	1.340(3)	C(14)-C(15)	1.503(4)
O(6)-C(20)	1.438(3)	C(14)-H(14)	1.0000
O(7)-C(9)	1.361(3)	C(15)-C(16)	1.430(4)
O(7)-C(21)	1.433(3)	C(16)-C(17)	1.345(3)
C(1)-C(2)	1.446(4)	C(16)-H(16)	0.9500
C(1)-C(12)	1.461(3)	C(18)-H(18A)	0.9800
C(2)-C(3)	1.354(3)	C(18)-H(18B)	0.9800
C(2)-H(2)	0.9500	C(18)-H(18C)	0.9800
C(3)-C(4)	1.461(3)	C(19)-H(19A)	0.9800
C(4)-C(5)	1.343(3)	C(19)-H(19B)	0.9800
C(4)-C(13)	1.466(3)	C(19)-H(19C)	0.9800
C(5)-C(6)	1.501(4)	C(20)-H(20A)	0.9800
C(5)-H(5)	0.9500	C(20)-H(20B)	0.9800
C(6)-C(14)	1.533(3)	C(20)-H(20C)	0.9800
C(6)-C(19)	1.536(4)	C(21)-H(21A)	0.9800
C(6)-C(7)	1.547(4)	C(21)-H(21B)	0.9800
C(7)-C(17)	1.519(3)	C(21)-H(21C)	0.9800
C(7)-C(8)	1.521(3)		

C(11)-O(2)-H(2A)	104(2)	C(3)-C(2)-C(1)	120.8(2)
C(3)-O(3)-C(18)	117.8(2)	C(3)-C(2)-H(2)	119.6
C(14)-O(4)-H(4)	105(2)	C(1)-C(2)-H(2)	119.6
C(17)-O(6)-C(20)	118.6(2)	O(3)-C(3)-C(2)	125.3(2)
C(9)-O(7)-C(21)	118.2(2)	O(3)-C(3)-C(4)	113.2(2)
O(1)-C(1)-C(2)	120.5(2)	C(2)-C(3)-C(4)	121.5(2)
O(1)-C(1)-C(12)	120.5(2)	C(5)-C(4)-C(3)	122.3(2)
C(2)-C(1)-C(12)	118.9(2)	C(5)-C(4)-C(13)	119.5(2)

C(3)-C(4)-C(13)	117.9(2)	O(4)-C(14)-H(14)	107.2
C(4)-C(5)-C(6)	122.3(2)	C(15)-C(14)-H(14)	107.2
C(4)-C(5)-H(5)	118.9	C(6)-C(14)-H(14)	107.2
C(6)-C(5)-H(5)	118.9	O(5)-C(15)-C(16)	122.9(3)
C(5)-C(6)-C(14)	110.9(2)	O(5)-C(15)-C(14)	119.7(2)
C(5)-C(6)-C(19)	109.4(2)	C(16)-C(15)-C(14)	117.4(2)
C(14)-C(6)-C(19)	109.0(2)	C(17)-C(16)-C(15)	120.9(3)
C(5)-C(6)-C(7)	109.3(2)	C(17)-C(16)-H(16)	119.6
C(14)-C(6)-C(7)	108.0(2)	C(15)-C(16)-H(16)	119.6
C(19)-C(6)-C(7)	110.2(2)	O(6)-C(17)-C(16)	125.0(2)
C(17)-C(7)-C(8)	110.69(19)	O(6)-C(17)-C(7)	111.1(2)
C(17)-C(7)-C(6)	112.0(2)	C(16)-C(17)-C(7)	123.9(2)
C(8)-C(7)-C(6)	110.4(2)	O(3)-C(18)-H(18A)	109.5
C(17)-C(7)-H(7)	107.9	O(3)-C(18)-H(18B)	109.5
C(8)-C(7)-H(7)	107.9	H(18A)-C(18)-H(18B)	109.5
C(6)-C(7)-H(7)	107.9	O(3)-C(18)-H(18C)	109.5
C(13)-C(8)-C(9)	118.7(2)	H(18A)-C(18)-H(18C)	109.5
C(13)-C(8)-C(7)	119.0(2)	H(18B)-C(18)-H(18C)	109.5
C(9)-C(8)-C(7)	122.2(2)	C(6)-C(19)-H(19A)	109.5
O(7)-C(9)-C(10)	123.3(2)	C(6)-C(19)-H(19B)	109.5
O(7)-C(9)-C(8)	115.7(2)	H(19A)-C(19)-H(19B)	109.5
C(10)-C(9)-C(8)	121.0(2)	C(6)-C(19)-H(19C)	109.5
C(11)-C(10)-C(9)	119.6(2)	H(19A)-C(19)-H(19C)	109.5
C(11)-C(10)-H(10)	120.2	H(19B)-C(19)-H(19C)	109.5
C(9)-C(10)-H(10)	120.2	O(6)-C(20)-H(20A)	109.5
O(2)-C(11)-C(10)	117.7(2)	O(6)-C(20)-H(20B)	109.5
O(2)-C(11)-C(12)	121.2(2)	H(20A)-C(20)-H(20B)	109.5
C(10)-C(11)-C(12)	121.0(2)	O(6)-C(20)-H(20C)	109.5
C(11)-C(12)-C(13)	118.2(2)	H(20A)-C(20)-H(20C)	109.5
C(11)-C(12)-C(1)	121.6(2)	H(20B)-C(20)-H(20C)	109.5
C(13)-C(12)-C(1)	120.2(2)	O(7)-C(21)-H(21A)	109.5
C(8)-C(13)-C(12)	121.5(2)	O(7)-C(21)-H(21B)	109.5
C(8)-C(13)-C(4)	119.5(2)	H(21A)-C(21)-H(21B)	109.5
C(12)-C(13)-C(4)	119.0(2)	O(7)-C(21)-H(21C)	109.5
O(4)-C(14)-C(15)	112.6(2)	H(21A)-C(21)-H(21C)	109.5
O(4)-C(14)-C(6)	109.7(2)	H(21B)-C(21)-H(21C)	109.5
C(15)-C(14)-C(6)	112.6(2)		

Anisotropic displacement parameters ($Å^2 \times 10^3$) for minimoidione A (**1**). The anisotropic displacement factor exponent takes the form: $-2\pi^2 [h^2 a^{*2} U^{11} + ... + 2 h k a^* b^* U^{12}]$

	U^{11}	U^{22}	U^{33}	U^{23}	U^{13}	U^{12}
O(1)	32(1)	22(1)	41(1)	-3(1)	13(1)	0(1)
O(2)	38(1)	19(1)	41(1)	2(1)	17(1)	-2(1)
O(3)	34(1)	35(1)	27(1)	1(1)	16(1)	-5(1)
O(4)	29(1)	41(1)	59(2)	13(1)	7(1)	-14(1)
O(5)	40(1)	35(1)	67(2)	22(1)	19(1)	-5(1)
O(6)	22(1)	25(1)	34(1)	2(1)	7(1)	-1(1)
O(7)	35(1)	26(1)	25(1)	-3(1)	16(1)	-5(1)
C(1)	17(1)	23(1)	29(2)	0(1)	3(1)	2(1)
C(2)	22(1)	29(2)	23(1)	-2(1)	7(1)	2(1)
C(3)	16(1)	32(2)	22(1)	3(1)	6(1)	2(1)
C(4)	20(1)	23(1)	24(1)	3(1)	7(1)	0(1)
C(5)	21(1)	25(1)	31(2)	6(1)	8(1)	-4(1)
C(6)	24(2)	23(1)	28(2)	-2(1)	5(1)	-7(1)
C(7)	24(1)	21(1)	19(1)	-1(1)	6(1)	-4(1)
C(8)	17(1)	21(1)	20(1)	2(1)	1(1)	-1(1)
C(9)	21(1)	24(1)	16(1)	1(1)	3(1)	-2(1)
C(10)	24(2)	24(1)	21(1)	4(1)	7(1)	-4(1)
C(11)	19(1)	17(1)	26(1)	4(1)	3(1)	-2(1)
C(12)	18(1)	20(1)	23(1)	2(1)	3(1)	0(1)
C(13)	16(1)	23(1)	18(1)	2(1)	1(1)	0(1)
C(14)	31(2)	24(2)	35(2)	-5(1)	10(1)	-10(1)
C(15)	31(2)	20(1)	44(2)	-1(1)	14(2)	-4(1)
C(16)	28(2)	26(2)	38(2)	7(1)	10(1)	1(1)
C(17)	25(2)	22(1)	26(2)	-5(1)	8(1)	-4(1)
C(18)	33(2)	49(2)	26(2)	-2(1)	12(1)	-3(1)
C(19)	29(2)	37(2)	36(2)	5(1)	3(1)	-8(1)
C(20)	24(2)	35(2)	49(2)	8(1)	6(1)	2(1)
C(21)	44(2)	38(2)	33(2)	-6(1)	22(2)	-11(1)

Hydrogen coordinates ($\times 10^4$) and isotropic displacement parameters ($Å^2 \times 10^3$) for minimoidione A (**1**).

	x	y	z	U(eq)
H(2A)	8440(30)	6238(18)	9473(17)	38
H(4)	4500(40)	651(13)	9330(20)	54
H(2)	6485	5132	11622	30
H(5)	5264	2478	10105	31
H(7)	7530	2270	7924	26
H(10)	9580	4993	7842	28
H(14)	5905	1025	8213	36
H(16)	9497	1000	10470	37
H(18A)	6460	4147	12880	53
H(18B)	5097	3475	12810	53
H(18C)	4717	4367	12173	53
H(19A)	3661	2516	7887	54
H(19B)	4671	2240	7164	54
H(19C)	4824	3195	7646	54
H(20A)	11585	1901	10950	56
H(20B)	12534	2221	10206	56
H(20C)	11658	1310	9989	56
H(21A)	9661	4115	6480	54
H(21B)	10576	3217	6613	54
H(21C)	11126	3942	7509	54

Hydrogen bonds for minimoidione A (**1**) [Å and °].

D-H...A	d(D-H)	d(H...A)	d(D...A)	<(DHA)
O(2)-H(2A)...O(1)	0.859(10)	1.784(16)	2.585(3)	154(3)
O(4)-H(4)...O(5)	0.860(10)	2.17(3)	2.692(3)	119(3)
O(4)-H(4)...O(5)#1	0.860(10)	2.11(2)	2.802(3)	138(3)

Symmetry transformations used to generate equivalent atoms:

#1 -x+1,-y,-z+2